Chemical Engineering Science 125 (2015) 32–57

Contents lists available at ScienceDirect

Chemical Engineering Science

journal homepage: www.elsevier.com/locate/ces

# Electrohydrodynamic atomization: A two-decade effort to produce and process micro-/nanoparticulate materials

Jingwei Xie [a,*], Jiang Jiang [a], Pooya Davoodi [b], M.P. Srinivasan [b], Chi-Hwa Wang [b,**]

[a] Department of Pharmaceutical Sciences and Mary & Dick Holland Regenerative Medicine Program, University of Nebraska Medical Center, Omaha, NE 68198, United States

[b] Department of Chemical and Biomolecular Engineering, National University of Singapore, Singapore 117585, Singapore

## HIGHLIGHTS

- Extensive investigation of EHDA in the past two decades.
- Production of micro-/nanoparticulate materials with well-controlled properties.
- Generation of desired patterns/structures through jet writing or deposition.
- Biomedical applications including drug delivery and regenerative medicine.
- Understanding the mechanism of EHDA using modeling and simulation techniques.

## GRAPHICAL ABSTRACT

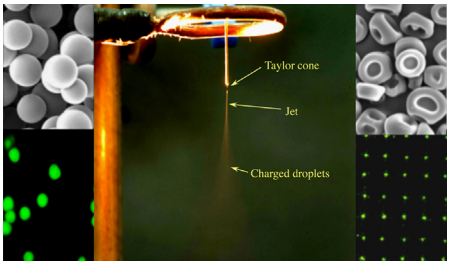


## ARTICLE INFO

*Article history:*
Received 5 June 2014
Received in revised form
15 August 2014
Accepted 30 August 2014
Available online 16 September 2014

*Keywords:*
Electrohydrodynamic atomization
Micro-/nanoparticles
Fabrication
Drug delivery
Regenerative medicine
Modeling

## ABSTRACT

Electrohydrodynamic atomization (EHDA), also called electrospray technique, has been studied for more than one century. However, since 1990s it has begun to be used to produce and process micro-/nanostructured materials. Owing to the simplicity and flexibility in EHDA experimental setup, it has been successfully employed to generate particulate materials with controllable compositions, structures, sizes, morphologies, and shapes. EHDA has also been used to deposit micro- and nanoparticulate materials on surfaces in a well-controlled manner. All these attributes make EHDA a fascinating tool for preparing and assembling a wide range of micro- and nanostructured materials which have been exploited for use in pharmaceutics, food, and healthcare to name a few. Our goal is to review this field, which allows scientists and engineers to learn about the EHDA technique and how it might be used to create, process, and assemble micro-/nanoparticulate materials with unique and intriguing properties. We begin with a brief introduction to the mechanism and setup of EHDA technique. We then discuss issues critical to successful application of EHDA technique, including control of composition, size, shape, morphology, structure of particulate materials and their assembly. We also illustrate a few of the many potential applications of particulate materials, especially in the area of drug delivery and regenerative medicine. Next, we review the simulation and modeling of Taylor cone–jet formation for a single and co-axial nozzle. The mathematical modeling of particle transport and deposition is presented to provide a deeper understanding of the effective parameters in the preparation, collection and pattering processes. We conclude this article with a discussion on perspectives and future possibilities in this field.



* Corresponding author. Tel.: +1 402 559 9442; fax: +1 402 559 7521.
** Corresponding author. Tel.: +65 6516 5079; fax: +65 6779 1936.
*E-mail addresses:* jingwei.xie@unmc.edu (J. Xie), chewch@nus.edu.sg (C.-H. Wang).

http://dx.doi.org/10.1016/j.ces.2014.08.061
0009-2509/

## 1. Introduction

The phenomenon of electrohydrodynamic atomization (EHDA), also simply called electrospray, was firstly observed and recorded by William Gilbert in 1600 (Gilbert et al., 1600). In 1750, Jean-Antoine (Abbé) Nollet, a French Clergyman and physicist, reported the earliest observation on electrospray, more than two centuries before the terminology was generated, demonstrating water flowing from a container would aerosolize if the container was electrified and put close to electrical ground (Dumont and Cole, 2013). Around one century later, Lord Kelvin invented a setup composed of two liquid nozzles that were bridged to opposite collection reservoirs and demonstrated small differences in charging between water dripping from the nozzles instantly caused differences in kilovolt scale and electrospraying from the nozzles (Smith, 2000). In 1882, Lord Rayleigh theoretically evaluated the charge that a liquid droplet could carry to the greatest extent, known as the "Rayleigh limit", which was confirmed experimentally 100 years later (Taylor, 1964; Gomez and Tang, 1994 and Duft et al., 2003). The first patent related to EHDA setup appeared in 1900 (Cooley, 1900). Zeleny conducted the electrospray experiment with ethanol and photographed a cone–jet in 1914 (Zeleny, 1917). In 1960s, Taylor developed a mathematical description of the EHDA process, simulating the conical shape of the liquid phase in the presence of an electrical field that became known as Taylor cone later on (Taylor, 1966). In the 1980s, Fenn and coworkers performed a series of studies that eventually made electrospray capable of introducing dissolved analytes into the gas phase for mass analysis (Fenn, 1989). John Bennett Fenn won the Nobel Prize in Chemistry in 2002 because of his contribution to electrospray ionization for analyzing biological macromolecules (Grayson, 2011).

EHDA is a well-practiced technique for generating very fine droplets with mono-dispersed size from a liquid under the influence of electrical forces. Though the applications of EHDA to many fields are numerous, including raindrops in thunderclouds, combustion, crop spraying, and electrospray ionization mass spectroscopy, this technique has started attracting a lot of attention since 1990s for producing and processing micro-/nanoparticulate materials in a rich variety of applications. In the present work, we begin with describing the basic setup and mechanism of EHDA, followed by a discussion of controlling composition, size, shape and secondary structure, collection, and deposition of micro-/nanoparticulate materials and their applications in the biomedical fields.

## 2. Electrohydrodynamic atomization: principles and basic setup

The basic setup for EHDA consists of several major components: a syringe pump, a syringe, a metal needle serving as nozzle, a high voltage power source and a grounded substrate serving as a collector (Fig. 1a). Some EHDA setups employ a closed chamber where air/nitrogen flow transfers particles toward collecting filters. The use of the chamber reduces the evaporation of solvents and facilitates formation of smaller particles with smoother surface morphology (Xie et al., 2006b, 2008b).

EHDA (electro refers to electric energy; hydrodynamic refers to fluid dynamics applied to liquids; and atomization refers to making bulk liquid into fine droplets) is a process where a liquid jet breaks up into fine droplets under influence of an external

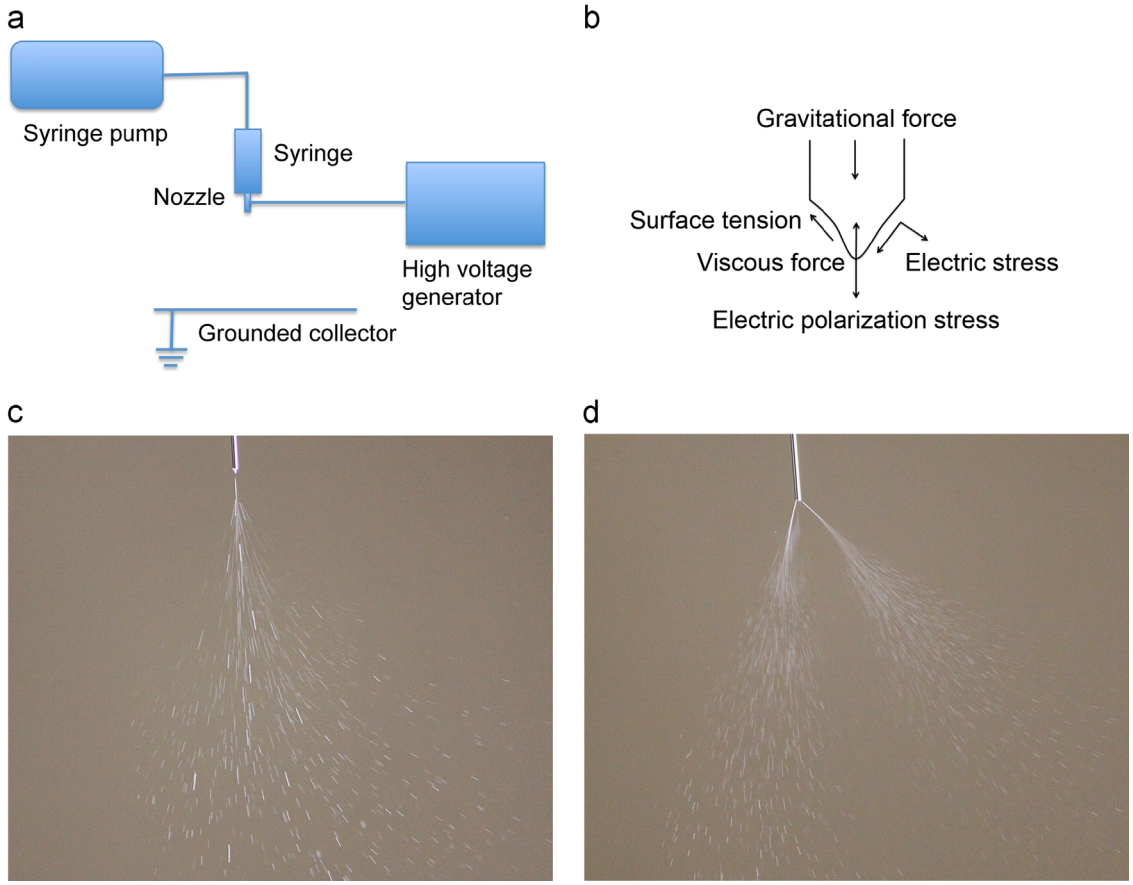


**Fig. 1.** Schematic illustration of (a) basic setup of EHDA and (b) major forces on the spraying cone (reprinted from Hartman et al., 1999, with permission from Elsevier). Photographs showing (c) a single-cone spraying mode (also called stable cone–jet mode) and (d) a multiple-cone spraying mode. (For interpretation of the references to color in this figure legend, the reader is referred to the web version of this article.)

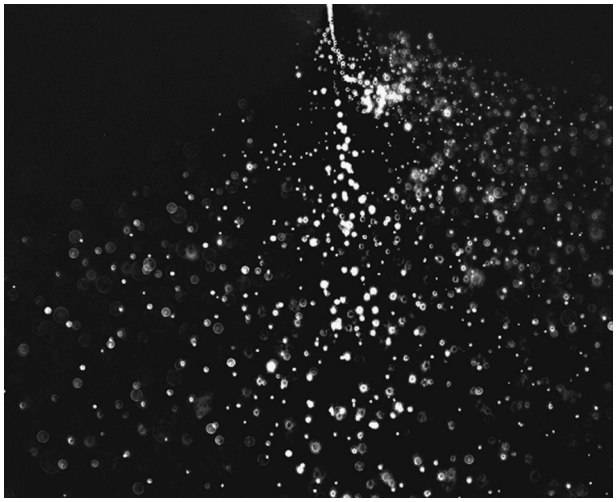

**Fig. 2.** High-speed video camera image showing a single-cone spraying mode (reprinted from Xie et al., (2008b), with permission from Elsevier).

electrical field. Different spraying modes that are observed (e.g. dripping, microdripping, simple-jet, single cone spraying (stable cone–jet), and multiple cone spraying) are determined by the competition of the electric stress and the surface tension stress on the liquid–gas interface and by the kinetic energy of the liquid leaving the nozzle (Fig. 1b–d). Under the observation of the naked eye, the jet appears in a mist form. A high speed video camera image of a single cone spraying reveals that the jet breaks up into fine droplets near the tip of nozzle due to varicose instability or kink/whipping instability when the electric normal stress overcomes the surface tension stress (Fig. 2) (Hartman et al., 2000; Camelot et al., 1999). Two videos are provided in the supplementary information showing both electrospraying and electrospinning jets. These video presentations provide complete illustration of jet breakup, droplet formation, and jet bending/whipping (Supplementary Information videos 1 and 2). After the droplets are emitted from the tip of the nozzle, they may undergo different scenarios: small droplet ejection, also called Rayleigh disintegration or Coulomb fission occurs; solvent evaporation increases the solute and charge concentrations; the reactive gas infiltrates the solution; and colloidal reactions occur within the solution (Salata, 2005). The maximum charge of a droplet is given by Eq. (1a) (Rayleigh, 1882). Normally, the solute in the droplet solidifies and forms micro- or nanoparticulate materials after the solvent evaporates if the amount of charge carried by the droplet is under Rayleigh disintegration limit ($L_r$) expressed in Eq. (1b) (Rayleigh, 1882).

$$q_R = 8\pi\varepsilon^{1/2}\gamma^{1/2}r^{3/2} \tag{1a}$$

$$L_r = (64\pi^2\varepsilon\gamma r^3)q_R \tag{1b}$$

where $q_R$ is the surface charge of a droplet, $\varepsilon$ is the dielectric constant of the liquid, $\gamma$ is the liquid surface tension and $r$ is the droplet radius.

Supplementary material related to this article can be found online at http://dx.doi.org/10.1016/j.ces.2014.08.061.

## 3. Criteria for EHDA

EHDA occurs as electric stress overcomes surface tension. Surface tension and electric conductivity of solvents play a critical role in EHDA. A liquid with surface tension higher than $5.0\times10^{-2}$ N m$^{-1}$ cannot be atomized in air by electric forces (Smith, 1986). Therefore, organic solvents are often used in EHDA as they usually possess low surface tension. The selection of proper solvents to dissolve polymers for electrospraying is a critical step, since the surface morphology of generated particles is highly dependent on the solvent's physicochemical properties. In general, electrospraying a polymer solution with a solvent with low vapor pressure and consequently high boiling temperature (e.g. N, N-dimethylformamide (DMF)) results in particles with smaller size and smoother surface morphology, however, it may also yield a bimodal size distribution due to weaker polymer chain entanglement. In contrast, solvents with high vapor pressure, low boiling temperature, and consequently faster evaporation rate (e.g. dichloromethane (DCM)) may result in the formation of textured and/or highly porous surfaces, and even hollow structures. In fact, the fast solvent evaporation rate reduces the time that polymer chains require to re-arrange within the droplet during rapid solidification (Bock et al., 2012).

Due to its high surface tension, EHDA of water or aqueous solutions may generate coronal discharge (e.g. electrical break down) in the air. Thus, inert gas environments (e.g. $CO_2$, Ar, and $N_2$) or vacuum is often required for EHDA of water (Tang and Gomez, 1994. During EHDA process, charges are transferred/immobilized to the surface of cone and jet thus causing jet break-up. Herein, conductivity or dielectric constant of liquid also plays an important role. Previous studies showed the conductivity of liquids could range from $10^{-11}$ to $10^{-1}$ S m$^{-1}$ when the liquid was operated in the cone–jet mode (Smith, 1986; Drozin, 1955). However, the conductivity with a range of $10^{-4}$ to $10^{-8}$ S m$^{-1}$ is generally considered for EHDA in this mode. In order to keep EHDA in the stable cone–jet mode, a minimum flow rate is known to scale as Eq. (2) when electrospraying low viscous liquids in the "high-conductivity" limit (Barrero, 2007).

$$Q_{min} \sim \frac{\varepsilon_r\gamma}{\rho K} \tag{2}$$

where $Q_{min}$ is the minimum flow rate, $\gamma$ is the surface tension of the working liquid, $\rho$ is the density of liquid, $K$ is the conductivity of liquid, and $\varepsilon_r$ is the permittivity of the working liquid.

Most recently, Scheideler and Chen (2014) examined the minimum flow rate scaling of highly viscous systems and obtained

$$Q_{min} \sim \frac{\gamma D^2}{\mu} \tag{3}$$

where $D$ is the diameter of spraying nozzle, and $\mu$ is the viscosity of fluid.

Previous studies also demonstrated that both DC and AC high voltages were suitable for EHDA (Borra et al., 1999b; Yeo et al, 2005).

## 4. Composition

It appears that EHDA can be used to fabricate and process particular materials without limiting the raw materials. Materials produced and processed by EHDA have been categorized as follows and summarized in Table 1.

### 4.1. Natural polymers

Natural polymers are commonly non-toxic and environmentally responsive via degradation and remodeling via enzymes secreted by cells due to their intrinsic property. Many natural polymers have been processed into particulate materials using EHDA. Here, we illustrate several notable examples.

#### 4.1.1. Chitosan

Chitosan is a linear, semi-crystalline natural polysaccharide composed of a randomly distributed (1→4)-2-acetamido-2-deoxy-β-D-glucan (N-acetyl D-glucosamine) and (1→4)-2-amino-2-deoxy-β-D-glucan (D-glucosamine) units, which can be readily

**Table 1**
List of materials produced and processed by EHDA.

| Materials | Sizes | Solvents | References |
|---|---|---|---|
| *Pharmaceutics/drugs* | | | |
| Aspirin | ≈ 6 μm | Ethanol | Li et al. (2006) |
| Methylparahydroxybenzoate | 1.58–4.55 μm | Ethanol | Ijsebaert et al. (2001) |
| Beclomethasone dipropionate | 1.5–4.5 μm | Ethanol | Ijsebaert et al. (2001) |
| Paclitaxel | ≈ 10 μm | Ethanol | Unpublished |
| Carbamazepine | 0.32–1.75 μm | Methanol | Wang et al. (2012) |
| Indomethacin | 1.7 μm | Ethanol | Nystrom et al. (2011) |
| Piroxicam | 5.5 μm | Chloroform | Nystrom et al. (2011) |
| Budesonide | 4.9 μm | Chloroform | Nystrom et al. (2011) |
| Niflumic acid | 0.2–0.8 μm | Acetone/water | Ambrus et al. (2013) |
| *Biological materials* | | | |
| Insulin | 110 nm | Ethanol/water/HCl | Gomez et al. (1998) |
| BSA | 700 nm | Ethanol/acetic acid | Tavares Cardoso et al. (2011) |
| Sucrose ($C_{12}H_{22}O_{11}$) | 20 nm | Water | Morozov (2011) |
| Sericin | 25–175 nm | DMSO | Hazeri et al. (2012) |
| Silk–elastin-like protein | 24 and 36 nm | Ammonium acetate buffer | Anumolu et al. (2011) |
| DNAs | | Water | Chen et al. (2000), Okubo et al. (2008) |
| Cells | | | Abeyewickreme et al. (2009), Ng et al. (2011), Sahoo et al. (2010), Braghirolli et al. (2013) |
| Whole organism | | | Mongkoldhumrongkul et al. (2010), Clarke and Jayasinghe (2008) |
| *Natural polymers* | | | |
| Chitosan | 124 nm and ≈ 2.5 μm | Ethanol/acetic acid/water | Arya et al. (2009), Pancholi et al. (2009), Zhang and Kawakami (2010) |
| Cellulose | ≈ 1 μm | Ethanol and butanone/DCM | Huang et al. (2012), Bodnar and Rosell-Liompart (2013) |
| Alginate | 0.15–2 mm | Water | Moghadam et al. (2008), Xie and Wang (2007), Tabeei et al. (2012), Park et al. (2012a) |
| *Synthetic polymers* | | | |
| PS | ≈ 0.75–5 | THF | Fantini et al. (2006) |
| PCL | 0.3–20 μm | DCM/chloroform/DMAc | Ding et al. (2005), Wu and Clark (2007), Enayati et al. (2010), Bock et al. (2011) |
| PLGA | 0.06–15 μm | DCM/acetonitrile/TFE/DMSO/TEAF | Xie et al. (2006a), Xie et al. (2006b), Almeria et al. (2010), Almeria and Gomez (2014), Berkland et al. (2004) |
| PLA | 3.7–19 μm | 1-Butanol/methylene chloride/1,2-dichloroethane-ethanol (DCE)/chloroform | Yeo et al (2005), Xu et al. (2006), Ikeuchi et al. (2012) |
| *Polymer/polymer blends* | | | |
| PLA/PLGA | ≈ 5 μm | DCM–DMSO | Xie et al. (2008a, b) |
| PLGA/Pluronics | ≈ 1.4–1.6 μm | THF–DMF | Seth and Katt (2012) |
| *Drug/polymer* | | | |
| Taxol/PCL | 3–10 | DCM–Acetonitrile | Ding et al. (2005) |
| Paclitaxel/PLGA | 17–32 | DCM–Acetonitrile | Xie et al. (2006b), Naraharisetti et al. (2007), Ranganath et al. (2009a, 2009b) |
| Beclomethasone-dipropionate/PLA | 230–850 nm | DCM–Ethanol | Valo et al. (2009) |
| Celecoxib/PLGA | 2–8 μm | Acetonitrile | Bohr et al. (2012) |
| Ketoprofen/ethyl cellulose | | Ethanol aqueous | Huang et al. (2012) |
| Piperine/p-coumaric acid–thiolated-chitosan | 2–5 μm | Lactic acid | Pengpong et al. (2014) |
| Quercetin/PVP,SDS,sucralose | 1.3–1.8 μm | Dimethylacetamide–Ethanol | Li et al. (2014) |
| Griseofulvin/poly(methacrylic acid–co-methyl methacrylate) | | 1 μm | Zhang et al. (2011) |
| BSA/lysozyme/PLGA | ~20 μm | DCM–water | Xie and Wang (2007a) |
| Salbutamol-sulfate/PLA | 230–850 nm | DCM–Ethanol | Valo et al. (2009) |
| BSA/PCL–PPE–EA | 2–4 μm | Water–DCM | Wu et al. (2010b) |

**Table 1** (*continued*)

| Materials | Sizes | Solvents | References |
|---|---|---|---|
| Ovalbumin/calcium alginate | 1.0–1.5 μm | Water | Suksamran et al. (2013) |
| BSA/PDMS | 5–6 μm | Water–acetone | Pareta and Edirisinghe (2006) |
| Budesonide/PLGA | ~3 μm | Acetonitrile | Lee et al. (2010b) |
| Paclitaxel/suramin/PLLA/PLGA | 10–20 μm | DCM–ethyl acetate | Nie et al. (2010a, 2010b) |
| Doxorubicin/elastin-like polypeptide | 150–570 nm | Water | Wu et al. (2009b) |
| Imidazoquinoline/acetalated dextran or acetalated dextran/tween blends | ~2 μm | Trifluoroethanol/methanol/ethanol/1-propanol/1-b | Duong et al. (2013) |
| Irinotecan/acetalated dextran/PLGA | 8.4 μm | DMF | Rahmani et al. (2013) |
| Cisplatin/maleimide–PEG–PLGA | ~550 nm | Ether/methanol | Bai and Liu (2014) |
| Gemcitabine/folate–chitosan | 200–300 nm | | Xu et al. (2013b) |
| *DNA* | | | |
| pClKLux | | Ethanol–water–ethanoic acid | Davies et al. (2005) |
| Plasmid DNA/PEI | | | Wu et al. (2010a) |
| Oblimerson sodium/Genasense/lipoplex | 100–2500 nm | PBS/ethanol | Wu et al. (2009a) |
| pET30a-GFP plasmid/gold nanoparticles | 20–50 nm | Water | Lee et al. (2011b) |
| Adenovirus/alginate | < 150 μm | Water | Park et al. (2012a) |
| *Food* | | | |
| Chocolate (fat, sugar, lecinthin) | | Melt | Gorty and Barringer (2011), Luo et al. (2012) |
| Cocoa butter, coca butter equivalent, lauric butter | | Melt | Marthina and Barringer (2012) |
| Zein-curcumin | 175–900 nm | Aqueous-ethanol | Gomez-Estaca et al. (2012) |
| Stearic acid–ethylcellulose–Maltol | 10–100 nm | Ethanol | Eltayeb et al. (2013) |
| *Composites* | | | |
| Polystyrene/silica nanoparticles | 60–100 μm | Water | Moon et al. (2004), Shen et al. (2010) |
| $TiO_2$–PMMA | 0.25–1.87 μm | Diethylene glycol dimethyl ether | Yun et al. (2009) |
| CdSeS–poly(styrene-acrylate) | 500–1000 nm | DMF | Sun et al. (2011) |
| PVA–MMT/Ag | ~4 μm | DMF/THF | Park et al. (2012a, b), Park et al. (2011, 2013) |
| Polystyrene-block-ethylene oxide-quantum dots/iron oxide | 36–38 nm | Water | Duong et al. (2014) |
| *Metals* | | | |
| Sn–Bi | 5–50 nm | Melt | Yu and Hu (1997) |
| Au | 7.1 nm, 10.9 nm 14.9 nm | Water–methanol | Lenggoro et al. (2002) |
| Pd | 4.3 nm | Water–methanol | Lenggoro et al. (2002). |
| Al | 4–14 μm | Ether–ethanol | Wang et al. (2013a) |
| *Carbon* | | | |
| Carbon nanotubes | ~100 nm | Methanol | Jennerjohn et al. (2010), Kim et al. (2010 b), Wang et al. (2013a, b) |
| Graphene | ~1 μm | Water | Tian et al. (2013) |
| *Inorganic materials* | | | |
| $TiO_2$ | 10–20 nm | Ethanol | Park and Burlith (1996), Wang et al. (2005), Terada et al. (2012) |
| $TiO_2/ZrO_x$ | 110 nm 2–4 μm | 1-BuOH | Borra et al. (1999a), Camelot et al. (1999) |
| $CeO_2$ | 24.6 and 29.9 nm | Ethanol/diethylene glycol butyl ether | Oh and Kim (2007) |
| ZnS | 20–40 nm | Ethyl alcohol | Lenggoro et al. (2000) |
| $Ce_2O_3/TiO_2$ | 80–500 nm | | Mou et al. (2013) |
| $BiFeO_3$ | | | Du et al. (2011) |
| $Li_{4/3}Ti_{5/3}O_4$ | 10 nm | 2-propanol–acetic acid | Doi et al. (2009) |
| Nano-sized hydroxyapatite | | | Li et al. (2007) |
| *Gas* | | | |
| Microbubble (air) | < 10 μm | | Farook et al. (2007a, 2007b), Pancholi et al. (2007), Farook et al. (2009) |

*Abbreviations*: PLGA, poly(lactic-co-glycolic acid); PLA, polylactic acid; PCL, poly(ϵ-caprolactone); PHBV, poly(3-hydroxybutyrate-*co*-3-hydroxyvalerate); TEAF, triethyl ammonium formate.

obtained from the alkaline deacetylation of chitin. Chitosan is a polycation whose primary amino groups can be protonated at low pH ($pK_a \sim 6.5$) and exhibits remarkable antibacterial, mucoadhesive, analgesic, hemostatic, biocompatible, and biodegradable properties (Croisier and Jerome, 2013). Arya et al. (2009) reported the use of EHDA for the preparation of chitosan-based micro/nanospheres. They examined the influence of a series of parameters including applied voltage, needle size, concentrations of chitosan and acetic acid solutions, and the collecting distance on the particle formation. Similarly, Pancholi et al. (2009) examined the effects of viscosity and surface tension on particle diameter during electrospraying chitosan solutions. They demonstrated that chitosan particles with diameter of about 2.5 μm can be generated using a chitosan solution with a viscosity of around 80 mPa s and the particle size can reduce to 500 nm when on drying. In another study, Zhang and Kawakami (2010) fabricated chitosan solid micro- and nanoparticles by electrospraying chitosan/acetic acid solution in one-step. It was found that the solution viscosity and conductivity played critical roles on electrospraying behavior, e.g. high viscosity and/or low conductivity can lead to stable electrospraying. By adding certain amount of ethanol to chitosan/acetic acid solution, they were able to obtain chitosan particles with diameter of 124 nm. In addition, researchers have demonstrated the encapsulation of various drugs in electrosprayed chitosan particles. Songsurang et al. (2011) prepared doxorubicin (DOX)-loaded chitosan particles using tripolyphosphate (TPP) as a stabilizer during EHDA process. Under the optimized conditions, the size of DOX-chitosan particles obtained were around 300–570 nm in dry state or 530–870 nm in hydrated state for initial drug loadings of 0.25–1%. More recently, Choi et al. (2013) demonstrated the fabrication of bovine serum albumin (BSA)-loaded chitosan microspheres by electrospraying acetic acid solution containing chitosan and BSA into sodium carbonate solution. The sodium carbonate solution could render the microspheres insoluble and solidified through neutralization of chitosan acetate. The high encapsulation efficiency can be achieved owing to quick solidification of microspheres and the interactions between oppositely charged chitosan and BSA. In a different study, Gu et al. (2013) demonstrated the fabrication of pH responsive, mono-dispersed chitosan microspheres ($256 \pm 18$ μm) containing glucose oxidase nanocapsules, and recombinant human insulin by a one-step electrospraying of an aqueous chitosan solution (2% w/v) into a receiving container containing 50 mL of 5% TPP with gentle agitation.

#### 4.1.2. Cellulose

Ethyl cellulose (EC) is an inert and water-insoluble polysaccharide and its coatings are highly stable under storage. These properties make it a good candidate for sustained-release carriers. Huang et al. (2012) recently fabricated EC microparticles containing different amounts of a model drug ketoprofen (KET) for sustained release by electrospraying EC (15% w/v) and KET (50%, 33%, 20%, 9% w/w) co-dissolved ethanol solution. The crystalline drug was in an amorphous state after encapsulation in EC particles and chemical interactions between KET and EC were noticed. In addition, with increasing the amount of EC content, the release rate of KET dropped. In a separated study, Bodnar and Rosell-Liompart (2013) examined the fabrication of EC particles by electrospraying EC in butanone and dichloromethane (DCM) at different humidity levels. They obtained various morphologies of particles including flatter, pancake-shaped, with a corrugated or dimpled wall, arising from primary droplets.

#### 4.1.3. Alginate

Sodium alginate, the sodium salt of alginic acid, is obtained from brown marine algae. The sodium alginate solution with concentration of 1–3 w/v% is a non-Newtonian and viscous liquid. Electrospray of a highly viscous and non-Newtonian alginate solution was often in either pulsating jet model or dripping model. Alginate beads/microspheres are usually formed by electrospraying of sodium alginate solutions into an aqueous solution containing a crosslinking agent (e.g. $CaCl_2$). Moghadam et al. (2008) produced mono-sized spherical alginate beads with size ranging from 0.57 to 2 mm by electrospraying high viscous alginate solution. Xie and Wang (2007b) demonstrated the fabrication of uniform alginate microbeads having diameters ranging from 200 μm to 2 mm by performing electrospray in the dripping mode through an additional ring electrode. Tabeei et al. (2012) showed the use of a pulsating DC electric field for production of alginate beads in millimeter scale at a critical frequency could result in a narrow size distribution. In a separate work, Park et al. (2012a) examined different concentrations and flow rates for the production of alginate beads, indicating alginate beads with diameter less than 150 μm can be achieved using a low alginate concentration ($< 1.0$ wt%) and a low flow rate ($< 2$ ml $h^{-1}$).

### 4.2. Synthetic polymers

Synthetic polymers have a number of advantages comparing to natural polymers as they can be tailored for the desired mechanical properties and the required degree of degradation. Furthermore, synthetic polymers are often in low cost and a more reliable source of raw materials. Fabrication of polymeric particles by EHDA shows the potential to eliminate the drawbacks associated with emulsion-based techniques and to generate micro- and nanoparticles with reproducible loadings.

#### 4.2.1. Polystyrene

Polystyrene (PS) has been studied as a model polymer for producing micro- and nanoparticles using EHDA. Fantini et al. (2006) examined the effects of four different molecular weights of PS for production of micro- and nanoparticles, showing the low molecular weight PS easily led to non-fiber forming. They also found that the large quantity of solvent to be evaporated could result in irregular and rough beads when using the high molecular weight PS. In contrast, the lower amount of solvent to be evaporated when using the low molecular weight PS could result in formation of spheres with uniform dimensions and smooth surfaces. A different study showed electrospraying of off-the-shelf colloid PS nanospheres (360 nm and 720 nm) for the production of thick layers of tridimensional order (Coll et al., 2013).

#### 4.2.2. Poly(ε-caprolactone) (PCL)/poly(lactide) (PLA)/poly(lactide-co-glycolide) (PLGA)

PCL/PLA/PLGA have been electrosprayed into nano- and microparticles for applications in drug delivery as they are FDA-approved, biocompatible and biodegradable polymers. PCL is biodegradable polyester with semi-crystalline structure and glass transition temperature around $-60$ °C. However, hydrophobic nature of PCL would be the major constraint in the encapsulation of natural or synthetic macromolecules such as DNA, proteins, and peptides as well as hydrophilic small molecules (e.g. doxorubicin) (Woodruff and Hutmacher, 2010; Freiberg and Zhu, 2004). Ding et al. (2005) and Xie et al. (2006a) fabricated mono-dispersed PCL particles with diameters ranging from 1 to 32 μm by electrospraying a PCL and dichloromethane (DCM) solution using a glass chamber. Wu and Clark (2007) prepared PCL particles with a mean-size of $4 \pm 0.3$ μm and a porous microstructure by electrospraying a PCL and chloroform solution into an aqueous solution, regulating the evaporation rate of solvents during the fabrication process. Enayati et al. (2010) prepared PCL particles with diameters ranging from 300 nm to 4500 nm by jetting a solution in the presence of an electric field. They were able to

control the size and size distribution of the fabricated particles by systematically adjusting the operating parameters. Bock et al. (2011) demonstrated the fabrication of relatively uniform-sized PCL microspheres with narrow size distributions and the average sizes of particles ranged from 10 to 20 μm. They also showed a high polymer concentration combined with a high feeding rate could ensure electrospraying in the semi-dilute entangled regime and result in the production of uniform sized and reproducible solid spheres and elimination of fiber formation and offspring droplets.

In another set of studies, Xie et al. (2006a, b) systematically examined the effect of parameters on PLGA particle formation by EHDA and demonstrated controlled morphologies (spherical, disintegrated, red blood cell-like, donut-like, porous, hollow) and sizes (255 nm to 15 μm). Almeria et al. (2010) further examined the fabrication of PLGA microparticles with different morphologies (spherical, elongated, and with one or multiple fibers attached to the particle core) and reported possible mechanisms. More recently, the same group reported the electrospray synthesis of monodisperse PLGA (M.W. 11–136 kDa) particles in a broad diameter range (60 nm–2 μm) which was determined by main parameters including solution conductivity, flow rate and initial polymer volume fraction (Almeria and Gomez, 2014). However, the scale of flow rate used in this study was in microliter per hour and the production rate was low, which made this process less practical for applications. In a separate study, Berkland et al. (2004) obtained PLGA particles with sizes of 300 nm using flow-limited field-injection electrospraying (FFES) 5% w/v PLGA in acetonitrile at flow rate of 1 ml $h^{-1}$, indicating injection charge could be more efficient for inducing an ionic state in a solution of PLGA than the conventional electrospray setup.

PLA has properties similar to that of PLGA, but has more crystalline structure that is responsible for slower degradation. Therefore, it is an interesting candidate for long-term degradation and release applications (Nie et al., 2010a, b). Yeo et al. (2005) fabricated PLA (M.W. 6000–16,000) particles ($3.7 \pm 1.9$ μm) by AC electrospraying 5% w/v PLA dissolved in 20% 1-butanol and 80% methylene chloride mixture, demonstrating that the particles ejected possess neutral charge (unlike DC electrospray) and thus eliminating the chance of surface adsorption and destabilization of the encapsulated molecules because of electroporation and/or compound ionization. In another study, Xu et al. (2006) showed that 1,2-dichloroethane (DCE) was a more suitable solvent for electrospraying PLA than DCM. Ikeuchi et al. (2012) recently demonstrated the fabrication of PLA particles with high surface porosities due to phase separation by electrospraying 1% PLA chloroform solution containing 5% ethanol in a high humidity environment (90%).

### 4.3. Polymer blends

Polymer blends may provide an optimized combination of different activities. For example, natural polymers generally have poor mechanical properties but may present some biological functions. Synthetic polymers are usually mechanically stronger than natural polymers but lack biological functions. A mixture of natural and synthetic polymers could address this problem by integrating multiple desired properties, which can simultaneously have the superior physical properties and biological functions. However, few studies have examined the electrospraying of polymer blends. Xie et al. (2008b) prepared microparticles composed of PLA/PLGA blends. It was demonstrated that the microparticles composed of PLA/PLGA (30/70) blends could form core–shell structure due to phase-separation during the electrospraying process. In a different study, Seth and Katt (2012) reported the electrospraying of blends of Pluronics® with PLGA for simultaneous modulation of morphology from doughnut-shape to spherical shape and surface properties (e.g. surface charge, surface hydrophobicity, and surface chemistry) of PLGA microparticles.

### 4.4. Inorganic materials

Owing to their intriguing properties, many efforts have been devoted to the preparation of metal oxide particles in the 1–100 nm range. Nanoparticles made of metal oxides or compounds have been achieved by combining electrospray and sol–gel chemistry. Park and Burlith (1992, 1996) prepared nanoparticles of anatase ($TiO_2$) with sizes of 20 nm by pyrolyzing amorphous precursor particles generated by electrospraying a modified titanium alkoxide ethanol solution into a heated chamber. Wang et al. (2005) demonstrated a one-step synthesis of $TiO_2$ nanoparticles having diameter of around 10 nm by electrospraying pyrolysis of three different organic precursors including titanium tetraisopropoxide and water-soluble titanium sources TC-300® and TC-400®. Similarly, Terada et al. (2012) fabricated $TiO_2$ nano- and microparticles by electrospraying titanium (IV) bis(ammonium lactato) dihydroxide aqueous solutions followed by the pyrolysis at 300–500 °C. In addition to the fabrication of $TiO_2$ nanoparticles, electrospray has been used for processing $TiO_2$ nanoparticles. Modesto-Lopez and Biswas (2010) examined the effect of electrical conductivity of nano-suspensions in the formation of $TiO_2$ agglomerates and $TiO_2$ films with electrospray. Similarly, Xi et al. (2011) fabricated polydispersed and nearly spherical $TiO_2$ aggregates with 0.4-3 μm in diameter by electrospraying a colloidal dispersion of P25 $TiO_2$ nanoparticles. The similar methodology has been reported for the fabrication or processing of other types of inorganic particles including $ZrO_x$, $CeO_2$, ZnS, $BiFeO_3$, hydroxyapatite, Quantum dots, and $Li_{4/3}Ti_{5/3}O_4$/CNT (Borra et al., 1999a; Hyuncheol et al., 2007; Camelot et al., 1999; Oh and Kim, 2007; Lenggoro et al., 2000; Li et al., 2007; Du et al., 2011; Jennerjohn et al., 2010; Doi et al., 2009).

### 4.5. Composites

Incorporation of nanoparticles to polymeric matrices can enhance and/or render novel functionalities of composites due to the interaction between nanoparticles and polymer matrices.

Moon et al. (2004) reported a one-step synthetic method for the preparation of colloidal aggregates and their inverse structures by electrospraying an aqueous colloidal suspension containing polystyrene beads and silica nanoparticles. Similar work has been reported for the generation of soft polymer spheres/silica crystal balls (Shen et al., 2010). Yun et al. (2009) fabricated nonagglomerated and monodispersed $TiO_2$-poly(methyl methacrylate) (PMMA) composite microspheres with a mean diameter ranging from 0.25 to 1.87 μm using a combination of beads mill and electrospray techniques. Sun et al. (2011) fabricated quantum dot (CdSeS QDs)-encoded poly(styrene-acrylate) microspheres by electrospraying the mixture of polymer solution and quantum dots solution, providing many reliable codes for multiplex detection. In different studies, Park et al. (2011, 2012b, 2013) demonstrated the fabrication of PVA/MMT, PVA/Ag, and PVA/MMT/Ag composite particles using electrospray and explored the test of antibacterial activity against *Staphylococcus aureus*. In addition, a more recent study demonstrated the fabrication of micellar (polystyrene-block-ethylene oxide) nanocomposites containing quantum dots (QDs), superparamagnetic iron oxide nanoparticles (SPIONs) and their combination via co-axial electrospray (Duong et al., 2014).

### 4.6. Metals

EHDA has been used for the production and processing of metal particles. Yu and Hu (1997) fabricated Sn–Bi nanoparticles with sizes from around 5 to 50 nm by electrospraying a master alloy of Sn-60 wt pct Bi eutectic prepared by vacuum melting. Kandjani et al. (2010) prepared metal particles with various shapes including tear drop, tad pole, oval like, ligament, dumbbell and irregular/splat by electrospraying Sn (60%)/Pb (40%) alloy melt into a viscous medium – transformer

oil. Other than fabrication of metal particles, electrospray was used for sizing metal particles. Lenggoro et al. (2002) showed that electrospray in conjunction with aerosol analyses (a differential mobility analyzer and a condensation nucleus/particle counter) can provide a means for sizing gold and palladium nanoparticles. Electrospray was also used to assemble metal particles. Wang et al. (2013a) generated a gel within a droplet via evaporation induced rapid aggregation of aluminum nanoparticles by co-axial electrospray, which contains a small mass fraction of nitrocellulose serving as an energetic binder and to adjust the particle size and morphology.

### 4.7. Carbon

Carbon nanotubes commonly tend to form bundles and are difficult to form aerosols in a well-controlled fashion because of their unique geometry and van der Waals forces. Jennerjohn et al. (2010) developed an approach for producing aerosols of carbon nanotubes in an occupationally relevant mass concentration—180 μg of nanotubes per cubic meter of the carrier gas using electrospray. A similar approach was carried out to disperse and aerosolize carbon nanofiber colloidal suspensions for in vitro and in vivo studies (Kim et al., 2010b; Wang and Pui, 2013). In addition, 2D nanoscale graphene building blocks were integrated into 3D structures using electrospray-assisted self-assembly. Tian et al. (2013) fabricated erythrocyte-like grapheme microspheres in high quality and mass production capability by electrospraying graphene oxide suspension into a coagulation bath (e.g. CTAB solution) followed by hydrazine hydrate reduction.

### 4.8. Drugs

It is reported that more than 95% of new drug candidates are associated with limited bioavailability due to their large size, low solubility and high crystallinity. Electrospray has been used to fabricate various pharmaceutical particles to reduce the size, increase the solubility, and generate the amorphous form normally adopted to improve bioavailability and administration of such drugs. Ijsebaert et al. (2001) prepared methylparahydroxybenzoate (MPHB) and beclomethasone dipropionate (BDP) particles with desired sizes ranging from 1.58 μm to 4.55 μm for inhalation purposes by electrospraying MPHB and BDP ethanol solutions. In order to reduce the size and obtain a regular shape of aspirin powder for inhalation applications, Li et al. (2006) produced aspirin particles with sizes less than 10 μm by electrospraying a saturated solution of aspirin in ethanol. Nystrom et al. (2011) investigated the formation of indomethacin, piroxicam and budesonide particles (1.7–5.5 μm) by electrospraying them in ethanol and chloroform at reduced pressure. It was found that electrospraying of a high volatile solution in a reduced pressure could lead to generation of more amorphous particles than electrospraying in atmospheric pressure, which was most probably attributed to the fast solidification. Scholten et al. (2011) fabricated carbamazepine (CBZ)-microparticles (a poorly water-soluble drug) of different sizes and shapes by controlling jet formation and breakup, droplet evaporation and solidification during electrospraying solutions containing different amounts of CBZ in DCM. In a separate study, Wang et al. (2012) demonstrated the production of crystals of CBZ with sizes ranging from $320 \pm 48$ nm to $1756 \pm 458$ nm via EHDA followed by annealing at high temperatures. In order to reduce the size, electrospray crystallization was used for the production of submicron-sized niflumic acid (NIF) crystals (200–800 nm), an anti-inflammatory drug, which is much smaller than the conventional NIF (around 80 μm) (Radacsi et al., 2012; Ambrus et al., 2013). Fu et al. (2012) prepared pharmaceutical particles containing both budesonide and epigallocatechin gallate due to charge-enhanced coagulation via customized bipolar electrospray setup. Other than pure drug solutions, additives together with drugs were also electrosprayed to form particulate formulations. Kawakami (2012) employed electrospray to prepare particulate formulations of drugs/polymeric excipients such as CBZ/poly(vinyl pyrrolidone) and prednisolone (PDN)/Eudragit. It was found that the excess amount of CBZ readily forms a pure crystalline phase due to phase separation when the poly(vinyl pyrrolidone) excipient was loaded with larger than 40% CBZ. In contrast, excess PDN can retain the amorphous state for an even higher loading.

### 4.9. Biological materials

EHDA has also been used to fabricate protein and enzyme nanoparticles. Gomez et al. (1998) showed the possibility of generating relatively uniform and biologically active insulin nanoparticles with a mean diameter around 110 nm by electrospraying insulin in mixed solvents containing 89.1–9.9–1 ethanol–water–4% molar HCl by volume. Morozov (2011) designed a nano-aerosol generator with an opposite electrospraying of volatile solvents for neutralization. The prepared bovine serum albumin (BSA) nanoparticles had mean diameters from $80 \pm 20$ nm to $115 \pm 15$ nm. In addition, Morozov (2011) also showed the fabrication of alkaline phosphatase (an enzyme) nanoparticles using a customized bipolar electrospray setup. It was shown that enzymes aerosolized by bipolar electrospray could maintain their specific bioactivity. Anumolu et al. (2011) generated hollow silk–elastin-like protein polymeric nanoparticles ($24.0 \pm 1.2$ nm and $36.0 \pm 1.4$ nm) and demonstrated precise control over their dimensions using a commercially available electrospray aerosol generator (TSI 3480) together with a differential mobility analyzer (DMA-TSI 3085). Hazeri et al. (2012) demonstrated the production of sericin nanoparticles with average particle sizes of 25–175 nm consisting of small crystallites and exhibiting a high moisture absorbance by electrospraying the sericin sponge in dimethyl sulfoxide.

EHDA has also been demonstrated as an intriguing approach for plasmid DNA delivery. Chen et al. (2000) examined the co-axial electrospraying of enhanced green fluorescent protein (GFP) plasmid for the delivery to African Green Monkey fibroblast cells. Okubo et al. (2008) showed that the charged water droplets generated from EHDA can produce temporary holes in cell membranes facilitating DNA transport into a living cell and the number of infected cells increased with increasing the applied voltage. In addition to biological molecules, living cells (immortalized cell line, primary cells, and stem cells) and organisms have been processed by EHDA. Ng et al. (2011) demonstrated the formation of functional cardiac tissues by electrospraying the three major cell types in the myocardium. Abeyewickreme et al. (2009) showed that the cellular viability and the pluripotency for mouse embryonic stem cells after electrospraying were indistinguishable when comparing with untreated cells. Sahoo et al. (2010) examined the effects of electrospraying process on the survival rate, growth, and multi-lineage differentiation potential of bone marrow stem cells (BMSCs). It was found that cells via electrospraying had a viability of approximately 88%, and their proliferation rate was similar to native BMSCs. Furthermore, BMSCs electrosprayed at 7.5 kV could differentiate into adipogenic, chondorgenic, and osteogenic lineages, indicating the retaining of their multipotency. Most recently, Braghirolli et al. (2013) also examined the survival rate, proliferation, DNA destruction, preservation of plasticity and the immunophenotypic profile of BMCS after electrospraying for 15–60 min. The study suggested that above 30 min of electrospraying caused DNA damage but the DNA was capable of repairing itself within 5 h. Mongkoldhumrongkul et al. (2010) demonstrated the non-parasitic nematode *Caenorhabditis elegans* – a well-characterized model organism subjected to electrospraying showed no modulation of the reproductive capability and no significant variations in stress-

response biomarkers like heat shock proteins. The same research group also demonstrated electrospraying of multicellular organisms such as zebrafish embryos (Clarke and Jayasinghe, 2008). The results from these studies indicated that the electrospraying process did not influence the cellular mechanisms essential for the development of a multicellular organism. Therefore, EHDA is quite a mild approach that can maintain the bioactivity of the majority of proteins and other fragile biological materials.

## 5. Size

The size of droplets directly determines the size of particles in EHDA. A number of scaling laws have been created for predicting the size of the droplets generated by EHDA in the cone–jet mode. In earlier studies, De La Mora and Loscertales (1994) obtained scaling laws for regular fluid as follows:

$$d_j \sim r^* = \left(\frac{Q\varepsilon\varepsilon_0}{K}\right)^{1/3} \tag{4}$$

where $d_j$ is the jet diameter, $r^*$ is a certain characteristic length, $Q$ is the liquid flow rate, $\varepsilon_0$ is vacuum permittivity, $\varepsilon$ is the permittivity of liquid, and $K$ is the conductivity of liquid.

Ganan-Calvo et al. examined high viscosity fluids with regular conductivity and obtained the scaling laws (Ganan-Calvo et al., 1997). For liquids with high enough conductivities and viscosities, the droplet size is approximately given by

$$\frac{d}{(\varepsilon-1)^{1/3}d_0} = 1.6\left[\frac{Q}{(\varepsilon-1)^{1/2}Q_0}\right]^{1/3} - 1.0 \tag{5}$$

$$d_0 = \left[\frac{\gamma\varepsilon_0}{\rho K^2}\right]^{1/3} \tag{6}$$

$$Q_0 = \gamma\varepsilon_0/\rho K \tag{7}$$

where $d$ is the diameter of droplet, $Q$ is the liquid flow rate, $\gamma$ is surface tension of the gas–liquid interface, $\varepsilon_0$ is vacuum permittivity, $K$ is the conductivity of liquid, and $\rho$ is the density of liquid.

For liquids with low conductivities and viscosities, the droplet size is approximately given by

$$\frac{d}{d_0} = 1.2\left(\frac{Q}{Q_0}\right)^{1/2} - 0.3 \tag{8}$$

Ganan-Calvo (1997) reported that the droplet diameter can be obtained by

$$d = 3.78\pi^{-2/3}Q^{1/2}\left(\frac{\rho\varepsilon_0}{\gamma K}\right)^{1/6} f_b \tag{9}$$

where $d$ is the droplet size, $\rho$ is the density of liquid, $\varepsilon_0$ is vacuum permittivity, $K$ is the conductivity of liquid, $\gamma$ is surface tension of the gas–liquid interface, and $f_b$ is the dimensionless radius of the jet at the breakup point ($f_b \approx 0.60$).

Hartman et al. (2000) reported the relationship between droplet size and variables in the cone–jet mode as follows:

$$I \propto (\gamma K Q)^{1/2} \tag{10}$$

$$d = C\left(\frac{\rho\varepsilon_0 Q^4}{I^2}\right)^{1/6} \propto Q^{1/2} \tag{11}$$

$$d \propto \left(\frac{1}{K}\right)^{1/6} \tag{12}$$

where $d$ is the diameter of droplet, $Q$ is the liquid flow rate, $I$ is the current transferred through the jet, $C$ is a constant, $K$ is the conductivity of liquid, and $\rho$ is the density of liquid.

Most recently, Ganan-Calvo et al. (2003) established the scaling laws for both the minimum flow rate obtained in the stable cone–jet mode of EHDA, and the droplet size achieved under that condition.

When viscous forces stall the jet emission before polarization forces, the jet diameter can be formulated as the following equation:

$$d_j = d_0\delta_\mu^{-1/2} \tag{13}$$

where $\delta_\mu = [\rho\varepsilon_0\gamma^2/K\mu^3]^{1/3}$ and $\mu$ is the viscosity of liquid.

When polarization forces rise against the main driver first, the jet diameter can be formulated as the following equation:

$$d_j = d_0\beta^{1/2} \tag{14}$$

where $\beta = \varepsilon/\varepsilon_0$

Table 2 represents a summary of scaling laws proposed for the calculation of droplet size and electrical current in EHDA.

By mass conservation, the droplet size is directly related to the particle size. One will be able to deduce Eq. (15) (Geerse, 2003) to relate final solid particle size ($dp$), initial droplet size ($d$), and weight fraction of solid material ($w$).

$$d_p = \left(\frac{\rho_s w}{\rho_s w + \rho_p(1-w)}d^3\right)^{1/3} \tag{15}$$

where $\rho_s$ and $\rho_p$ are the densities of the solvent and solid material.

So far, electrospray has been successfully applied to produce particles with sizes as small as around 10 nm. According to the scaling law, the flow rates applied were usually very low (in the scale of microliter per hour) in order to achieve particles with sizes less than 100 nm.

## 6. Morphology, shape, and secondary structure

The consolidation mechanism for electrosprayed droplets could be similar to that of spray drying. The difference is that electrosprayed droplets are usually smaller and carry charges on the surface, resulting in enhancement of the evaporation rate of solvents in electrosprayed droplets. Electrospray has been demonstrated capable of generating particles with various morphologies, shapes and secondary structures. Fig. 3 shows a schematic illustrating the possible morphologies, shapes and structures of particles that can be achieved using the different spraying nozzles. Almeria et al. (2010) extended a semi-empirical model that was originally developed to predict the transition from electrospray to electrospinning to evaluate the morphology of the particles generated by determining whether entanglements in the droplets are present in the Rayleigh limit (Shenoy et al., 2005). However, this approach failed to predict detailed morphological features but only distinguish spherical from non-spherical particles. To validate the model, Almeria et al. (2010) demonstrated the production of PLGA particles with different morphologies including spherical, tailed, and elongated. In a different study, Doshi et al. (2009) prepared red blood cell-like PLGA particles using two approaches: directly electrospraying and 2-propanol treatment to PLGA microspheres generated by EHDA. Park et al. (2011) fabricate polyurethane particles with disk, torus (red blood cell like), and spherical shapes. Semi-spherical hollow structures of silica nanocomposites, PMMA, and polystyrene were also obtained using EHDA (Deotare and Kameoka, 2006; Liu and Kumar, 2005; Lee et al., 2003). Chang et al. (2010a, b) demonstrated the fabrication of hollow and one-hole polymethylsilsesquioxane (PMSQ) microspheres with a controllable thickness by coaxial electrospraying PMSQ in the shell and perfluorohexane (PFH) in the core. In addition, polymeric particles with well-controlled porous structure can be produced by electrospray as well (Wu and Clark, 2007).

**Table 2**
Scaling laws for the prediction of droplet diameter in a single EHDA system.

| Droplet diameter | Current | Dimensionless parameters | References |
|---|---|---|---|
| $D_d \sim d_j \sim R^* = \left(\frac{\rho Q^2}{\gamma}\right)^{1/3}$<br>when $\eta \gg 1$ | $I = f(\varepsilon)(\gamma Q K/\varepsilon)^{1/2}$ | $\eta = \left(\frac{\rho K Q}{\gamma \varepsilon_0 \varepsilon}\right)^{1/2}$<br>$(0.51 \le \eta \le 2.01)$ | De La Mora and Loscertales (1994) |
| $D_d \sim d_j \sim r^* = \left(\frac{Q\varepsilon\varepsilon_0}{K}\right)^{1/3}$<br>when $\eta \sim 1$ | | | |
| $D_d = k_d Q^{1/2}\left(\frac{\rho\varepsilon_0}{\gamma K}\right)^{1/6}$<br>when $\beta \sim 1$ | $I = k_I\left(\frac{QK\varepsilon_0\gamma^3}{\rho}\right)^{1/4}$ | $\beta = \frac{\varepsilon}{\varepsilon_0}$ | Ganan-Calvo et al. (1994) |
| $D_d = k_d' \beta^{1/6}\left(\frac{Q\varepsilon_0}{K}\right)^{1/3}$<br>when $\beta \gg 1$ | $I = k_I'\left(\frac{QK\gamma}{\beta^{1/2}}\right)^{1/2}$ | | |
| $\frac{d}{(\varepsilon-1)^{1/3}d_0} = 1.6\left(Q/\left((\varepsilon-1)^{1/2}Q_0\right)\right)^{1/3} - 1.0$<br>$\delta_\mu \delta^{1/3} \ll 1$ | $I = 6.2\left(\frac{Q}{Q_0(\beta-1)^{1/2}}\right)^{1/2} - 2.0$ | $\delta_\mu \delta^{1/3} = \left(\frac{\varepsilon_0^2\gamma^3}{K^2\mu^3 Q}\right)^{1/3}$<br>$Q_0 = \gamma\varepsilon_0/\rho K$ | Ganan-Calvo et al. (1997) |
| $\frac{d}{d_0} = 1.2\left(\frac{Q}{Q_0}\right)^{1/2} - 0.3$<br>$\delta_\mu \delta^{1/3} \gg 1$ | $I/I_0 = 11.0\left(\frac{Q}{Q_0}\right)^{1/4} - 5.0$ | $I_0 = (\varepsilon_0\gamma^2/\rho)^{1/2}$<br>$d_0 = \left(\gamma\varepsilon_0^2/\rho K^2\right)^{1/3}$ | |
| $D_d = G(\kappa) r^*$<br>$G(\kappa) = -10.9\kappa^{-6/5} + 4.08\,\kappa^{-1/3}$ | $I = f(\kappa)(\gamma K Q/\kappa)^{1/2}$<br>$f(\kappa) = -499 - 0.21\kappa + 157\kappa^{1/6} + 336\kappa^{-1/6}$ | $\kappa$=dielectric constant<br>$r^* = (Q\varepsilon\varepsilon_0/K)^{1/3}$ | Chen and Pui (1997) |
| $d = 2 \times 1.89\, R_0 f_b$<br>$= 3.78\,\pi^{-2/3} Q^{1/2}\left(\frac{\rho\varepsilon_0}{\gamma K}\right)^{1/6} f_b$ | $I = 4.25\left(\frac{\gamma K Q}{\ln(Q/Q_0)^{1/2}}\right)^{1/2}$ | $Q_0 = \rho K/\gamma\varepsilon_0$ | Ganan-Calvo et al. (1997) |
| $\frac{d}{d_0} = k_d\left(\frac{Q}{Q_0}\right)^{1/2}$<br>$K_d$: constant; it depends on needle-to-electrode potential difference as well as on the needle radius. | $\frac{I}{I_0} = k_I\left(\frac{Q}{Q_0}\right)^{1/2}$<br>$k_I$: constant; it depends on needle-to-electrode potential difference as well as on the needle radius. | $d_0 = \left(\frac{\gamma\varepsilon_0^2}{\pi^2\rho K^2}\right)^{1/3}$<br>$I_0 = \left(\frac{\gamma\varepsilon_0^{1/2}}{\rho^{1/2}}\right)$ | Ganan-Calvo et al. (1997) |
| $d_d \sim \left(\frac{\rho\varepsilon_0 Q^3}{\gamma K}\right)^{1/6}$ | $I = (\gamma K Q)^{1/2}$ | The velocity profile in the jet is assumed to be flat | Hartman et al. (2000) |
| $D_d \sim d = \left(\frac{\rho\varepsilon_0 Q^3}{\gamma K}\right)^{1/6}$ | $I = (\gamma K Q)^{1/2}$ | Inertia and electrostatic suction scaling[a]:<br>$\alpha_\rho \gg \alpha_\mu^{1/4}$ and $\alpha_\rho/(\beta-1) \gg 1$ | Ganan-Calvo, (2004) |
| $D_d \sim d = \left(\frac{\rho\varepsilon_0 Q^3}{\gamma K}\right)^{1/6}$ | $\left(\frac{\rho K^2 Q^2}{(\beta-1)\varepsilon_0}\right)^{1/2}$ | Inertia and polarization forces scaling:<br>$1 \gg \frac{\alpha_\rho}{(\beta-1)} \gg \frac{\alpha_\mu}{(\beta-1)^4}$ | |
| $D_d \sim d = \left(\frac{\mu\varepsilon_0^2 Q^3}{\gamma K^2}\right)^{1/8}$ | $I = (\gamma K Q)^{1/2}$ | Viscous force and electrostatic suction scaling:<br>$\alpha_\rho \ll \alpha_\mu^{1/4}$ and $\alpha_\mu/(\beta-1)^4 \gg 1$ | |
| $D_d \sim d = \left(\frac{\mu Q}{(\beta-1)\gamma}\right)^{1/2}$ | $I = \left(\frac{\mu^3 K^3 Q^2}{(\beta-1)^4\gamma^2\varepsilon_0^2}\right)^{1/2}$ | Viscous force and polarization force scaling:<br>$\frac{\alpha_\rho}{(\beta-1)} \ll \frac{\alpha_\mu}{(\beta-1)^4} \ll 1$ | |

[a] $\alpha_\rho = \rho K Q/\gamma\varepsilon_0$; $\alpha_\mu = \mu^3 K^2 Q/\gamma^3\varepsilon_0^2$; $\beta$ is the liquid polarity parameter.

Loscertales et al. (2002) generated monodisperse capsules with diameters varying between 0.15 and 10 μm using steady coaxial electrospraying jets of immiscible liquids. Since then, various core–shell structured particles have been developed using the similar approach (Kazemi and Lahann, 2008; Xu et al., 2013a; Cao et al., 2014). The triple coaxial electrospraying device was also developed for the production of triple-layered structures in a single step process (Kim and Kim, 2010; Labbaf et al., 2013). In separate studies, multi-chamber microspheres were generated by utilization of a modified co-axial electrospraying device called compound-fluidic electrospray (Chen et al., 2008; Zhao and Jiang, 2009). In addition, Lahann's group demonstrated the fabrication of biphasic Janus particles and triphasic nanocolloids with nanoscale anisotropy by making use of side-by-side electrospraying (Roh et al., 2005, 2006, 2007; Bhaskar et al., 2008; Hwang et al., 2010; Lim et al., 2010; Yoshida et al., 2009; Lahann et al., 2011). This approach can be extended to the fabrication of multicompartmental particles including side-by-side, pie-shaped, asymmetric, striped, and rosette compartment configurations (George and Braun, 2009). Bicompartmental particles of different shapes including discs, rods, and spheres were also demonstrated via side-by-side electrospray (Bhaskar et al., 2010). Kazemi and Lahann (2008) also demonstrated the fabrication of core–shell microparticulate structures via side-by-side electrospraying of miscible polymer solutions using the same setup. Alternatively, Janus particles can be produced by bi-polar electrospraying (Mou et al., 2013).

## 7. Particle collection

Particles generated by electrospray were normally collected on the grounded substrate – a piece of aluminum foil in the laboratory. However, particles should be collected in a controllable way for practical applications. Ijsebaert et al. (2001) applied a gas flow to a glass chamber for inhalation purpose, demonstrating mass production rates ranging from 1.4 to 9.5 $\mu g\, l^{-1}$ air. Ding et al. (2005) used the similar setup for the production of PCL particles and they performed yield analysis for different operation and collection conditions. It was found that particles were deposited on the different parts including filter, inside wall, spray nozzle and ground needle and the total yield was less than 80%. After electrospraying, particles mainly endured electrical force (electrical field), drag force (air flow), columbic repulsive force (between particle), gravitational force (gravity) and buoyancy force (air). If particles were completely discharged, the particle trajectory can be easily controlled by the gas flow. Only a small fraction of particles were deposited on the filter, which could be due to incomplete discharge of particles. As a follow-up, the same group further improved the particle collection efficiency based on a modified setup (Rezvanpour et al., 2010). It was demonstrated that the particle collection efficiency was influenced by important factors presented in the following orders: solution flow rate, nitrogen flow rate, ring voltage, and nozzle voltage. The electric potential difference between nozzle and ring may also greatly influence the particle collection efficiency. The other factors affecting particle collection efficiency included durations of the process, polymeric materials, and electrical conductivities of solutions. The maximum collection efficiency can reach around 80% on the grounded aluminum collecting plate. They further performed the scaling analysis of this process for better control of pharmaceutical particle production (Rezvanpour et al., 2012). It was found that the electrical field and flow field forces played more important roles than the particle acceleration, gravitational and Saffman lift forces in their EHDA setup. An equation was also derived to describe the relation between a unique dimensionless group and the particle collection efficiency. They further investigated the effect of the

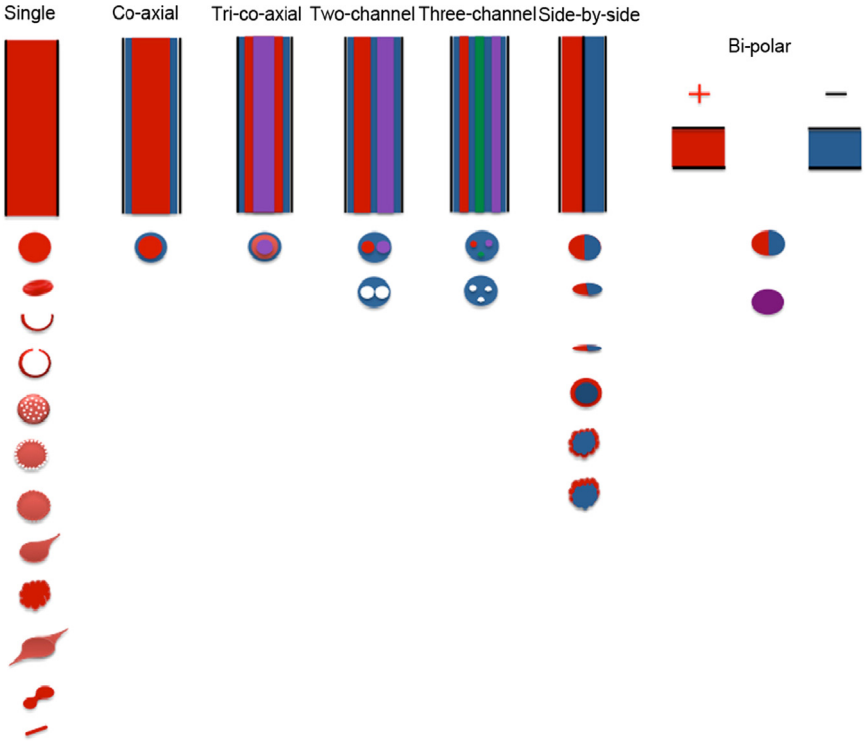


**Fig. 3.** Schematic illustration of various electrospraying nozzles (top) and possible morphologies and structures (bottom) of particles achieved using these spraying nozzles. The configurations of the nozzle include single spraying nozzle, co-axial nozzle, tri-co-axial nozzle, multiple-channel nozzle, side-by-side nozzle, and bi-polar nozzle. By making use of these nozzles, particles obtained can be spherical, red-blood cell shaped, hollow, multicompartmental, core–shell, tear-drop shaped, cup-shaped, porous, corrugated, and irregular shaped etc. (For interpretation of the references to color in this figure legend, the reader is referred to the web version of this article.)

auxiliary electric field formed by an additional flat plate connected to a high voltage supply and placed a few centimeters above the collecting plate on the particle collection efficiency (Rezvanpour and Wang, 2014). The collection efficiency can reach more than 90% in the optimized condition. In a different study, Grafahrend et al. (2010) developed a new and optimized electrospraying device consisting of the basic electrospray configuration, a spraying chamber, and a cyclone-type particle collector that can continuously produce 11.875 mg $h^{-1}$ monodisperse micro-sized particles with a yield of 79.2% while a basic electrospraying device allowed collection of only 34.7% of the generated particles.

## 8. Deposition

Based on the configurations, the types of electrospray deposition can be easily classified by traditional film/membrane deposition (Fig. 4a), droplet/particle placing (Fig. 4b), jet writing/printing (Fig. 4c), mask patterning (Fig. 4d), and electric field controlled deposition (Fig. 4e and f). We highlight some of them in the following paragraphs.

### 8.1. Direct jet writing (printing)

Electrospraying jet has been studied for printing or writing different materials on the surface for various applications. Chen et al. (2006) and Poon et al. (2008) showed "drop-and-place" particle deployment using a pulsed electrohydrodynamic jetting, demonstrating the capability of single particle manipulation and generation of linear colloidal crystal arrays. Samarasinghe et al. (2006) showed the deposition of gold nanoparticles to prepare conducting tracking on a table driven by a stepper motor using the electrohydrodynamic jet printing process. Lee et al. (2007) demonstrated the production of functional two-dimensional patterns of silver nanoparticles by making utilization of the silver nanocolloid jet that was generated in the cone–jet model of EHDA. Rahman et al. (2012) showed a fine-resolution patterning of copper nanoparticles on silicon substrate by electrohydrodynamic printing technology.

Park et al. (2007) demonstrated the printing of complex patterns of inks (e.g. insulating and conducting polymers, single-walled carbon nanotubes) by integrated computer-controlled electrohydrodynamic jet printer systems. The same group also demonstrated the formation of electrosprayed oligonucleotides nano-patterns for biosensing and nanomaterials assembly applications (Park et al., 2008). Galliker et al. (2011) demonstrated the direct printing of nanostructures by electrostatic autofocussing of ink nanodroplets and the generation of plasmonic nanoantennas with characteristic lengths as small as 50 nm. Korkut et al. (2008) showed the fabrication of polystyrene particle cluster arrays using an electrohydrodynamic printing system consisting of a motion system consisting of a rotary table and linear motor. Bodnar and Rosell-Liompart (2013) showed growth dynamics of ethyl cellulose granular films produced by electrospray deposition. Saywell et al. (2010) demonstrated the electrospray deposition of porphyrin polymers and oligomers on Au (1 1 1) surface, exhibiting a pattern of interdigitated chains from neighboring molecules. Electrohydrodynamic jetting has been used for depositing polymers and composites on different surfaces for biomedical applications (Ahmad et al., 2010; Nithyanandan et al., 2013).

Morozov and Morozova (1999) showed the electrospray deposition of alkaline phosphatase (AP) to produce protein films with active biological functions. It was found that protein inactivation upon electrospray is mainly determined by voltage and current applied. The inactivation of electrosprayed proteins could also be attributed to the humidity and the presence of protective substances in solutions. Their most recent study showed that the inactivation of jack bean urease occurred when the enzyme solution ( $< 20$ μg/ml) was electrosprayed at a current of 200 nA despite the low yield of the reactive oxygen species but the presence of 0.1 mM EDTA can retain the bioactivity of the electrosprayed urease (Kanev et al., 2014). Drop-on-demand patterning of bacterial cells on a nutrient-coated membrane and a raw silicon wafer in a straightforward, quick, and cost-effective manner was produced using electrohydrodynamic jet printing (Kim et al., 2009; Kim et al., 2010a, b).

### 8.2. Mask patterning

Morozov's group showed the preparation of single- and multicomponent microarrays of biologically active substances on any marginally conductive substrate (e.g. membrane, wet glass, semiconductor) using a dielectric mask (e.g. Teflon, mica, and nylon) with an array of holes during electrospray deposition (Morozov and Morozova, 1999; Avseenko et al., 2001, 2002; Morozov, 2010). In this case, the electric field is a superposition of an attracting electric field projecting through the holes and a repelling electric field of the mask charged with some amount of the deposited electrosprayed particles. Therefore, at the beginning of experiment, particles could be deposited on the mask, resulting in

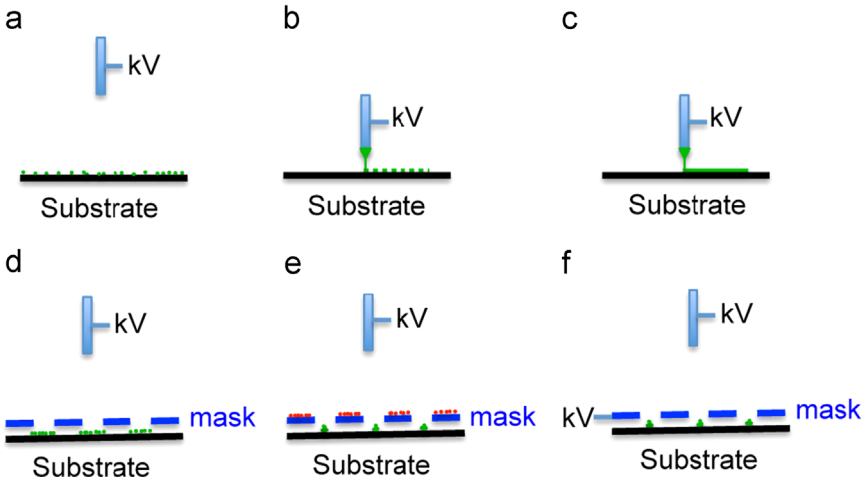


**Fig. 4.** Schematic illustrating different configurations of electrospray deposition. The pre-deposited ions on the mask are labeled in red (e). The deposited materials are labeled in green (a–f). (For interpretation of the references to color in this figure legend, the reader is referred to the web version of this article.)

loss of materials. Researchers further demonstrated the patterning of nano-sized hydroxyapatite and silicon-doped hydroxyapatite on both metallic (titanium) and non-metallic surfaces (glass) using a gold mesh mask during electrospray deposition (Li et al., 2008; Munir et al., 2011). Similarly, Higashi et al. (2014) demonstrated the electrospray deposition of micropatterned silica nanoparticles through a stencil mask. They also showed the deposition of silver nanoparticles on the patterned silica nanoparticles, resulting in strong surface-enhanced Raman scattering effects. It was shown that the pattern can be provided with accuracy greater than 95% for patterns with line widths greater than 50 μm when using a 20 μm thick mask made of nickel.

### 8.3. Electric field controlled deposition

Additional electric field has been used for the control of deposition of various materials during electrospray. Saf et al. (2004) demonstrated the fabrication of the thin films of functional organic materials by electrospray deposition to a moving target through a series of electrostatic lenses. Kim et al. (2006) developed an ion-induced parallel-focusing approach to pattern silver nanoparticles on both conducting (p-type silicon) and non-conducting (silica) surfaces through accumulating positive nitrogen ions generated by a corona discharger on the surface of the mask to form "focusing effect" similar to the electrostatic lens. In their following studies, they reported the parallel generation of nanoparticles (Ag, Cu, ZnO, PS) and protein (IgG) nanoarrays with 20–420 nm features as well as microarrays on various substrates (glass, PET film) using the same setup (Woo et al., 2011). They further demonstrated the generation of 3D assembly of nanoparticles with ordered arrays by extending electrospraying deposition time (Lee et al., 2011a). In a separate study, Xie et al. (2010) developed a simpler method to generate "electrostatic focusing effect" by directly applying a high voltage to the mask (Fig. 5). They demonstrated the fabrication of biodegradable and biocompatible polymeric particle patterns and subsequent formation of cell microarrays. The same group further developed a mathematic model to track the trajectories of particle and to better understand electrostatic focusing effect in the process of electrospray deposition on the substrate (Rezvanpour and Wang, 2011).

## 9. Applications

### 9.1. Pharmaceutical and food processing

Various pharmaceutics have been processed into micro- and nanoparticulate formulations using EHDA as mentioned above. In addition, EHDA technique has been used for food processing. Notable examples are as follows. Gorty and Barringer (2011) demonstrated that the electrospraying of chocolate a new approach allowing chocolate to be atomized due to the existence of an electric field can achieve a thin and even coating of chocolate. The same group also demonstrated confectionery coating (cocoa butter, coca butter equivalent, and lauric butter) using electrospray that offered greater and more complete coverage than non-electrospray coating (Marthina and Barringer, 2012). Luo et al. (2012) demonstrated the production of very fine, near-monodisperse chocolate particles by electrospraying chocolate suspensions. In a different study, Gomez-Estaca et al. (2012) examined the formation of zein nanoparticles and encapsulation of curcumin (a food coloring and active ingredient) in particles by EHDA. They further tested the performance of curcumin-loaded zein nanoparticles in semi-skimmed milk coloring, showing the potential of obtaining milk-based products with different shades and chromaticities through the addition of various amounts of curcumin-loaded zein nanoparticles. Additionally, Eltayeb et al. (2013) demonstrated the preparation of solid lipid nanoparticles

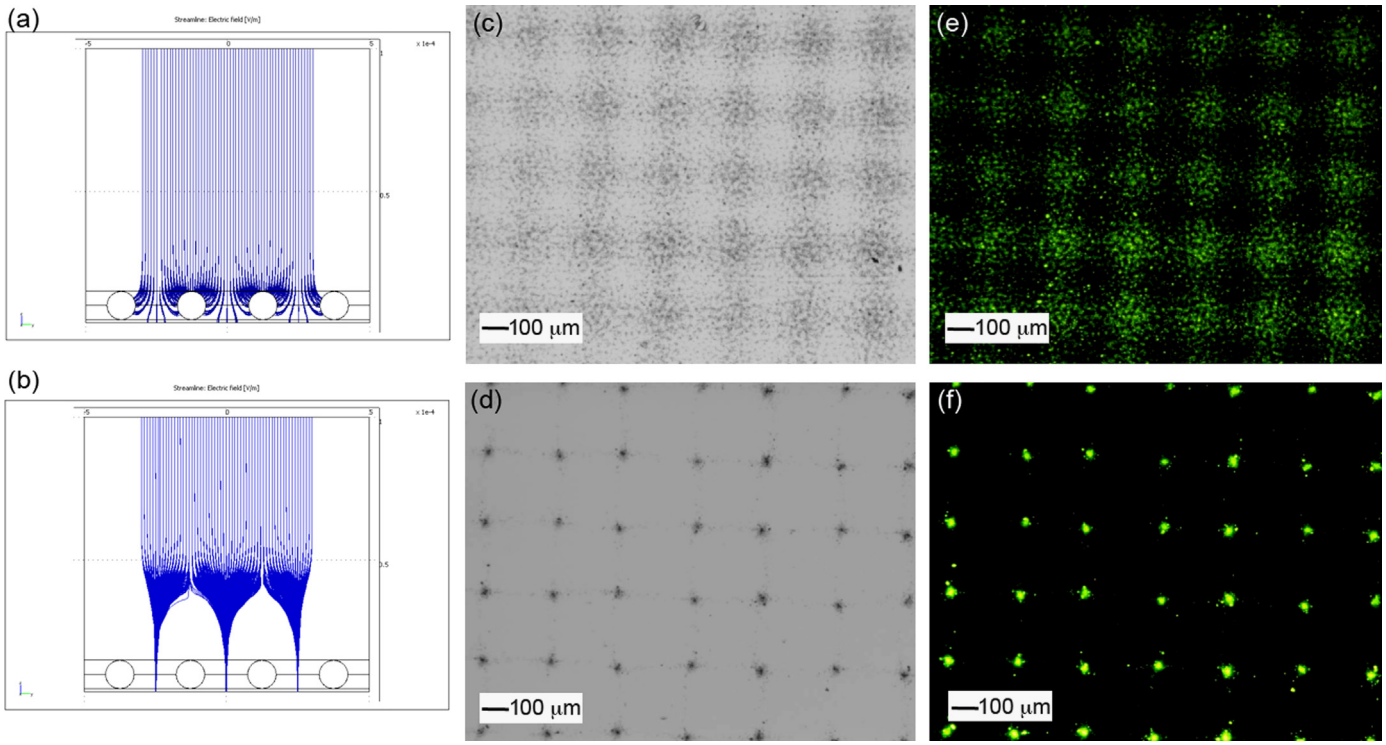


**Fig. 5.** (a, b) Computational simulation of electric field stream line (YZ projection) with 7.5 kV applied to the nozzle under different potential differences between mask and substrate: 0 V (a) and 2 kV (b). (c, d) Optical phase contrast and (e, f) fluorescence microcopy images of FITC-polystyrene nanoparticle patterns fabricated under different potential differences between mask and substrate: 0 V (c, e) and 2 kV (d, f) (reprinted from Xie et al., 2010. Copyright 2010 John Wiley & Sons, Inc.). (For interpretation of the references to color in this figure legend, the reader is referred to the web version of this article.)

(stearic acid (SA) and ethylcellulose (EC)) containing an active ingredient (Maltol) by electrospraying.

### 9.2. Drug/gene/virus delivery

EHDA is a promising technology for encapsulating both hydrophobic and hydrophilic drugs into polymeric particles (Bock et al., 2012). For hydrophobic drugs, they can be simply mixed with polymers and dissolved in organic solvents to form a solution that can be electrosprayed to form micro- and nanoparticles. Ding et al. (2005) and Xie et al. (2006a) demonstrated the encapsulation of paclitaxel – a hydrophobic drug in PCL and PLGA microparticles using electrospray, exhibiting sustained release of paclitaxel more than 30 days. Their subsequent study examined the performance of paclitaxel-loaded PLGA microparticles on the topical delivery of paclitaxel for the treatment of C6 glioma tumors inoculated subcutaneously in BALB/c nude mice (Naraharisetti et al., 2007). It was shown that microparticles with 20% drug loadings had good performance where the suppression of tumor growth was observed for about 10 days after the first administration. Comparing to other formulations (discs), microparticles generated by EHDA are normally more effective in suppressing tumor growth because of its inhibited burst release and the latter linearly sustained release. The same group developed a composite implant (calcium alginate beads) composed of paclitaxel-loaded PLGA microspheres embedded in alginate hydrogel matrix (Ranganath et al., 2009a, b). They further tested the implant using an intracranial U87 MG-luc2 glioblastoma model. The medium cross-linked calcium/alginate beads showed around 30 times higher anti-tumor growth activity and lower tumor proliferation index than sham and placebo controls after treatment for 41 days. In a different study, Valo et al. (2009) encapsulated beclomethasone-dipropionate a hydrophobic drug in PLA nanoparticles via electrospray in the stable cone–jet mode. Bohr et al. (2012) also fabricated celecoxib-loaded PLGA microparticles with diameters ranging from 2 to 8 μm for improving oral delivery where celecoxib is a hydrophobic, non-steroidal anti-inflammatory drug with a low aqueous solubility ( ≈ 5 μg/ml) and solubility-limited bioavailability. Ketoprofen (KET) a hydrophobic drug extensively used for treatment of inflammation, pain, or rheumatism was encapsulated in ethyl cellulose microparticles by electrospray (Huang et al., 2012). It was noted that the crystalline drug was transformed into an amorphous form in all the particles. More recently, Pengpong et al. (2014) encapsulated piperine a model hydrophobic drug in p-coumaric acid-thiolated-chitosan microparticles with an encapsulation efficiency of over 80%, exhibiting a sustained release of piperine up to 75% over 12 h between pH 1.2 and 6.4. In order to develop a fast-dissolving formulation for quercetin a poorly water-soluble drug, Li et al. (2014) prepared core–shell microparticles with PVP and quercetin in the core and PVP, SDS, and sucralose in the shell by co-axial electrospray. It was demonstrated that the rapid release, within one minute, of the incorporated quercetin from microparticles enhanced the permeation rates across the sublingual mucosa around 10 times faster than raw quercetin. Similarly, in order to improve oral absorption (e.g. solubility and bioavailability) of griseofulvin, which is an oral effective antifungal agent, Zhang et al. (2011) fabricated core–shell microparticles with griseofulvin in the core and poly(methacrylic acid–co-methyl methacrylate) (Eudragit L-100) in the shell using co-axial electrospray. This formulation showed much better dissolution and absorption behaviors, which could be due to the complete amorphization, smaller particle size, and improvement in dispersity.

For hydrophilic drugs, they can firstly be dissolved in an aqueous solution and subsequently mixed with polymer organic solvent solution to form an emulsion that can be electrosprayed to form drug-loaded polymeric micro- and nanoparticles or core–shell particles with drug in the core and polymer in the shell. BSA and lysozyme were encapsulated in PLGA microparticles through electrospraying an emulsion solution for sustained delivery (Xie and Wang, 2007a; Wang et al., 2013b). Similarly, Valo et al. (2009) showed encapsulation of salbutamol-sulfate in PLA nanoparticles via electrospray. In a different study, Wu et al. (2010b) produced core–shell microspheres with BSA as the core and poly(ε-caprolactone-polyamino-ethyl ethylene phosphate) (PCL–PPE–EA) an amphiphilic biodegradable polymer as the shell using a one-step electrospraying technology. The protein release profiles exhibited constant release for more than 3 weeks without a significant initial burst. Alternatively, the encapsulation of hydrophilic drugs can be realized by electrospraying the water solution formed by co-dissolving hydrophilic drugs and water-soluble polymer followed by cross-linking and/or coating. Suksamran et al. (2013) prepared calcium alginate microparticles incorporating ovalbumin as a model antigen followed by methylated N-(4-N,N-dimethylaminocinnamyl) chitosan coating, demonstrating mucosal immune response after oral administration in vivo. In order to increase the encapsulation efficiency, protect the drugs from degradation, and prolong the release period, hydrophilic drugs can be encapsulated in the core of core–shell micro- and nanoparticles generated by coaxial electrospray. Pareta and Edirisinghe (2006) fabricated core–shell microspheres with starch and BSA in the core and polydimethylsiloxane (PDMS) in the shell using coaxial electrospray, which can avoid exposing the proteins to toxic organic solvents that cause denaturation. Similarly, Xie et al. (2008a) showed the incorporation of BSA/lysozyme in PLGA microparticles via coaxial electrospraying of aqueous solution in the core and polymer solution in the shell. In a separate study, Wang et al. (2013b) compared the release kinetics of protein-loaded microparticles fabricated by either electrospraying emulsion or coaxial electrospray. They found that microparticles prepared by coaxial electrospray showed a greater decrease in the initial burst release and a significantly higher loading efficiency than the particles prepared by the emulsion electrospray. Lee et al. (2010b) fabricated budesonide-loaded PLGA particles having sizes in the range from 165 nm to 1.2 μm by coaxial electrospray. The particles had two features: the drug release profile for particles less than 1 μm is mainly due to the penetration of water and drug diffusion and the core–shell structure greatly reduces the burst release of drugs at the initial stage. The same research group also reported the fabrication of tri-layered composite particles with encapsulation of various drugs in different layers using tri coaxial electrospray (Lee et al., 2011b). It was shown that tuning the layer thickness and material composition of layers can more efficiently control the release profiles of encapsulated drugs (Fig. 6).

In addition to encapsulation of single drug, Nie et al. (2010a) prepared microspheres containing hydrophobic and hydrophilic drugs in the core and shell or vice versa via coaxial electrospray for sequential and concurrent release of different drugs. They subsequently fabricated core–shell PLLA–PLGA microparticles with encapsulation of paclitaxel and suramin in the core and shell or vice versa, which provided either a sequential release or parallel release (Nie et al., 2010b). They further tested the performance of microparticles in chemotherapy of U87 glioma a subcutaneous xenograft in BALB/c nude mice, demonstrating the higher dose of suramin released at the initial stage may efficiently suppress the tumor cell proliferation. In contrast, a subsequent sustained release of paclitaxel could enhance the apoptosis of tumor cells.

Other than traditional delivery systems, EHDA has been recently used to generate acid sensitive and targeted drug delivery systems. Wu et al. (2009b) showed the fabrication of doxorubicin-loaded elastin-like polypeptide (17.8 kDa) nanoparticles by EHDA. Such

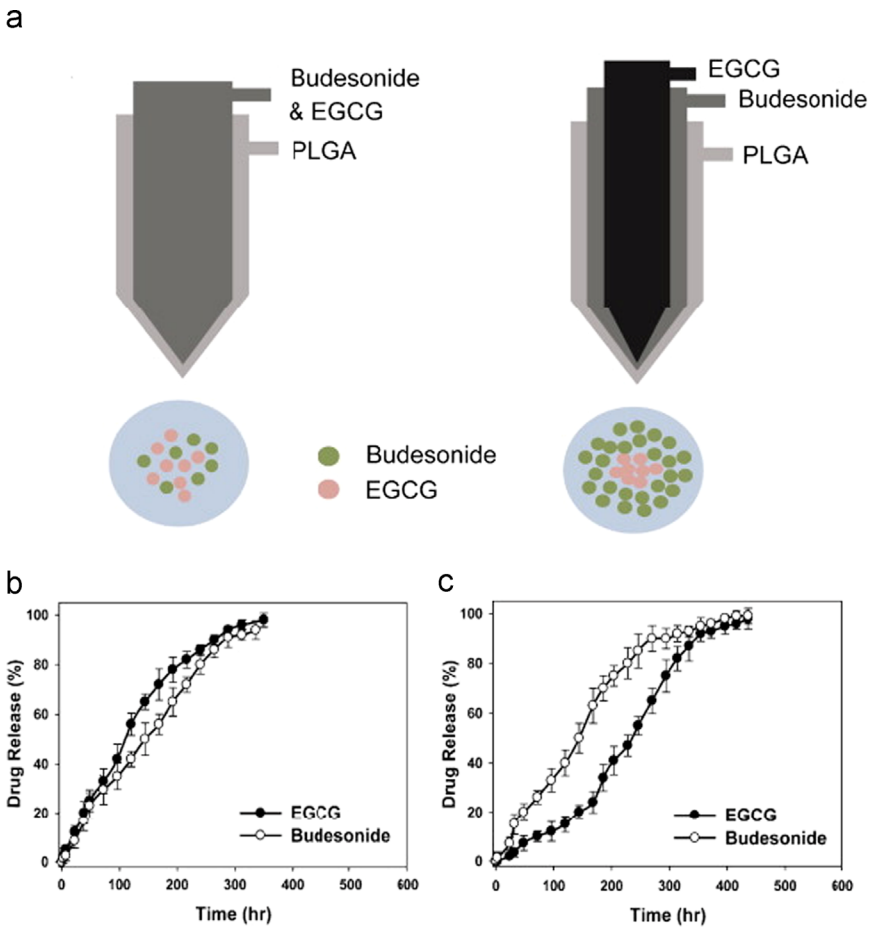


**Fig. 6.** (a) Schematic illustrating the co-axial and tri co-axial electrosprays and the corresponding microcapsules. The release profiles of PLGA-coated multidrug particles produced by co-axial electrospray (b) and tri co-axial electrospray (c) (reprinted from Lee et al., 2011b, with permission from Elsevier). (For interpretation of the references to color in this figure legend, the reader is referred to the web version of this article.)

particles showed pH-mediated release of doxorubicin. In a different study, Duong et al. (2013) demonstrated the encapsulation of the imidazoquinoline adjuvant resiquimod in microparticles made of acetalated dextran or acetalated dextran/tween blends that is acid responsive. It was shown that the drug released completely within 8 h under phagosomal condition and within 48 h under physiological condition because of the acid-responsive nature of acetalated dextran. The use of resiquimod-loaded particles can elicit much greater immune response in RAW macrophages than free drug. Further in vivo study suggested that intravenous injection of these microparticles into mice inoculated with Leishmania can significantly eliminate parasite load in the bone marrow versus controls. Rahmani et al. (2013) investigated the pH-responsive delivery of irinotecan from microparticles having two different compartments generated by side-by-side electrospray. Bai and Liu (2014) prepared cisplatin-loaded maleimide–PEG–PLGA particles using EHDA and subsequently conjugated with CD44 antibody. The resultant particles demonstrated a higher cell-killing outcome against ovarin cancer cells as compared to free form of cisplatin and particles without such antibody conjugation. The proposed antibody-functionalization strategy demonstrated a viable approach for producing particles with targeting ability in cancer therapy. Alternatively, Xu et al. (2013b) demonstrated the fabrication of core–shell nanoparticles with gemcitabine in the core and folate–chitosan in the shell for potential tumor-targeted, pH sensitive drug delivery by coaxial electrospray. The in vitro release profiles suggested a regulated burst release at the initial stage followed by a sustained release lasting for 3 days under neutral and acidic conditions, and the drug-releasing rate was higher under the acidic condition. In addition, the folate conjugated core–shell nanoparticles showed high particle uptake efficiency specifically by pancreatic cancer (BXPC3) cells, indicating the targeting potential.

EHDA was also reported for use in gene delivery. Davies et al. (2005) started investigating gene delivery using mice upon exposure to naked pCIKLux aerosols produced by EHDA though the efficiency was greatly compromised compared to the use of pDNA/PEI polyplexes (Koshkina et al., 2003). Wu et al. (2010a) demonstrated the production of plasmid DNA/polyethylenimine (PEI) polyplexes by coaxial electrospray. The delivery efficiency of these polyplexes was 2.6-fold higher than that generated by bulk mixing when the nitrogen to phosphate ratio (N/P) was 6.7. The same research group also prepared oligodeoxynucleotide G3139 (oblimerson sodium or Genasense)-loaded lipoplex nanoparticles that can efficiently deliver G3139 to K562 cells and downregulate the bcl-2 protein expression by $34 \pm 6\%$ and $57 \pm 3\%$ (Wu et al., 2009a). In a different study, Lee et al. (2011c) developed a method for delivering genes to microorganism *Escherichia coli* cells via electrospraying a mixture of pET30a-GFP plasmid and nano-sized gold particles. The momentum of gold nanoparticles attributed to the electric field can promote the delivery of DNA plasmids to microbial hosts and greatly enhance the transformation efficiency. In addition, Park et al. (2012a) fabricated calcium alginate beads for the delivery of adenovirus using EHDA, showing the high-efficiency transduction of cancer cells by the released adenovirus from the alginate beads.

### 9.3. Imaging contrast agent

EHDA has been used to produce contrast agents for various imaging applications. The utilization of microbubbles as contrast agents for the delineation and perfusion of tissues evokes a great deal of interest in ultrasound imaging. Edirisinghe's group first demonstrated the fabrication of microbubble suspensions containing uniform bubbles smaller than 10 μm in size based on co-axial electrospray (Farook et al., 2007a, b). The same research group further prepared phospholipid-coated microbubble suspensions with diameters of 3–7 μm (Pancholi et al., 2007; Farook et al., 2009). They found these bubbles had high structural stability and their size remained almost the same for 160 min at room temperature. However, the mean bubble diameter decreased dramatically and then became stable at around 1–2 μm after 20 min under the human body temperature. Unfortunately, there is no report on in vivo studies of microbubbles generated by this technique. In separate studies, EHDA has been applied to encapsulate magnetic nanoparticles in polymeric materials for magnetic resonance imaging (MRI). Kim et al. (2013) encapsulated magnetic nanoparticles in polysorbate 80 by co-axial electrospraying of magnetic particles in hexane in the core and polysorbate 80 in the shell. Similarly, Gun et al. (2013) encapsulated superparamagnetic iron oxide nanoparticles within PLGA microspheres by co-axial electrospray, demonstrating the potential use as transverse relaxation contrast agents in MRI. Recently, electrospray was also used to fabricate micellar nanocomposites containing quantum dots, superparamagnetic iron oxide nanoparticles, and their combination, presenting potential for fluorescence and MR imaging (Anthony et al., 2014). In addition, particles fabricated by electrospray may present multimodalities for imaging and therapeutic applications. Hayashi et al. (2010) produced red blood cell-like particles having dual-modality including magnetic resonance and fluorescence imaging using EHDA. Low-temperature magnetic measurements confirmed the superparamagnetic behavior of the particles. The particles showed an obvious dark contrast in MRI and an effective fluorescence. In another study, Misra et al. (2012) fabricated multicompartmental particles encapsulated with gold nanostructures and siRNA having functions of both near infrared imaging and siRNA delivery (Fig. 7). Fig. 7a shows a schematic illustrating the bicompartmental particles with functions of both imaging and siRNA delivery. Fig. 7b shows a fluorescent image of bicompartmental particles. The blue and red colors indicate PLGA portion and a composite portion composed of PLGA/crosslinked PEI incorporated with rhodamine-labeled siRNA, respectively. Fig. 7c shows the release kinetics of siRNA from bicompartmental particles. Fig. 7d shows that the particles with dual functions were capable of silencing GFP production in 48 h. Si et al. (2012, 2013) also demonstrated the loading of drugs and imaging agents in PLGA microparticles, indicating the potential of co-axial electrospray for encapsulation of different drugs and imaging agents within microparticles for multimodal diagnosis and imaging-guided treatment.

### 9.4. Cell/tissue encapsulation and regenerative medicine

The encapsulation of living cells within a semi-permeable matrix protecting transplanting non-autologous cells from the host immune system could be used in drug and cell delivery, immunotherapies and engineering tissue constructs. EHDA shows great potential for the encapsulation of living cells in the microbeads. Xie and Wang (2007) demonstrated the production of uniform alginate beads with sizes ranging from 200 μm to 2 mm under high flow rates using a modified electrospray setup. The encapsulation of HepG2 cells in alginate beads was also demonstrated. Young et al. (2012) examined the effect of operating parameters such as flow rates and applied voltages on the diameter and uniformity of the

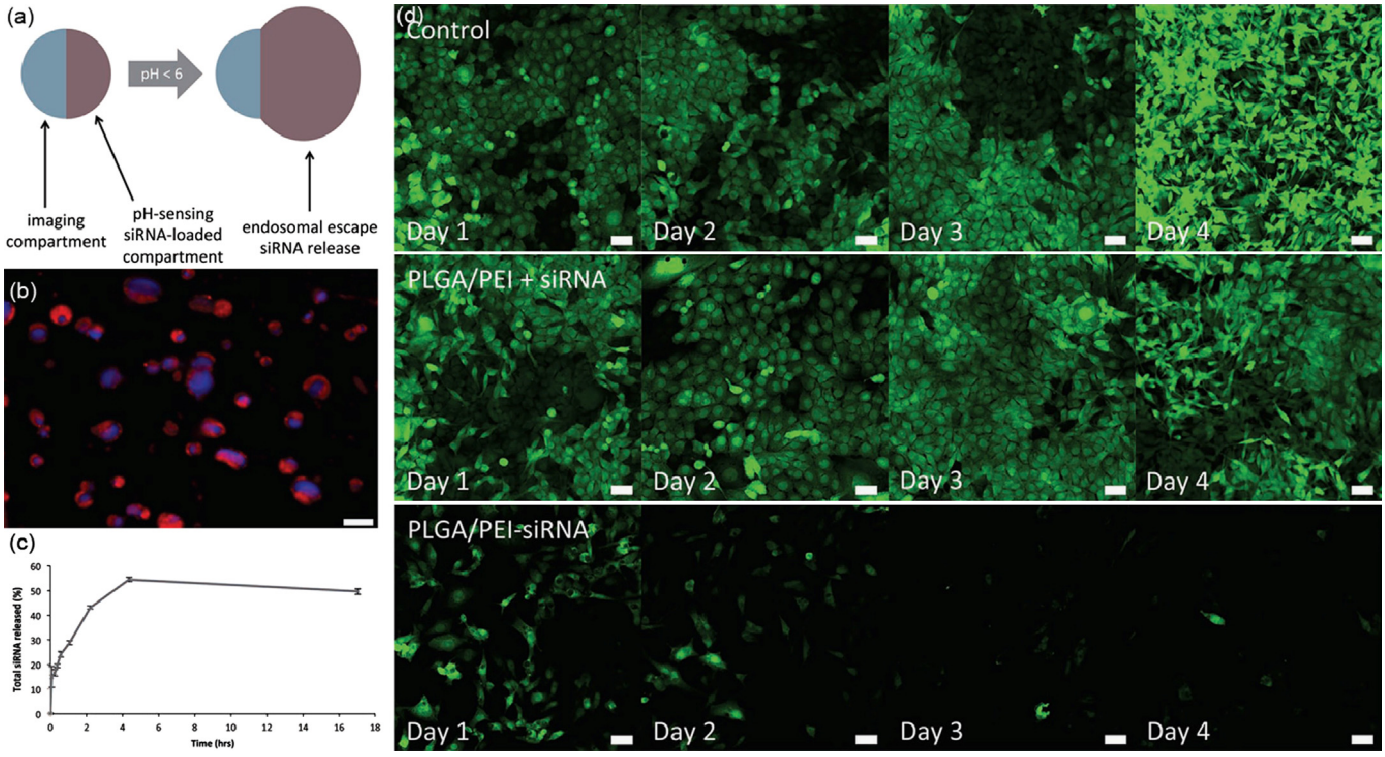


**Fig. 7.** Multicompartmental particles for combined imagine and siRNA delivery: (a) bicompartmental particles illustrating different compartments with complimentary functions-imaging and siRNA delivery. (b) Fluorescent image of bicompartmental particles with blue fluorescent PLGA imaging compartment and a composite PLGA/crosslinked PEI compartment loaded with rhodamine-labeled siRNA. (c) siRNA release kinetics. (d) In vitro particles incubation experiments with MDA-MB-231/GFP breast cancer cells. Control: without treatment. PLGA/PEI+siRNA: particles and soluble siRNA. PLGA/PEI-siRNA: siRNA-loaded particles. Scale bar=50 μm (reprinted from Misra et al., 2012. Copyright 2012 John Wiley & Sons, Inc.). (For interpretation of the references to color in this figure legend, the reader is referred to the web version of this article.)

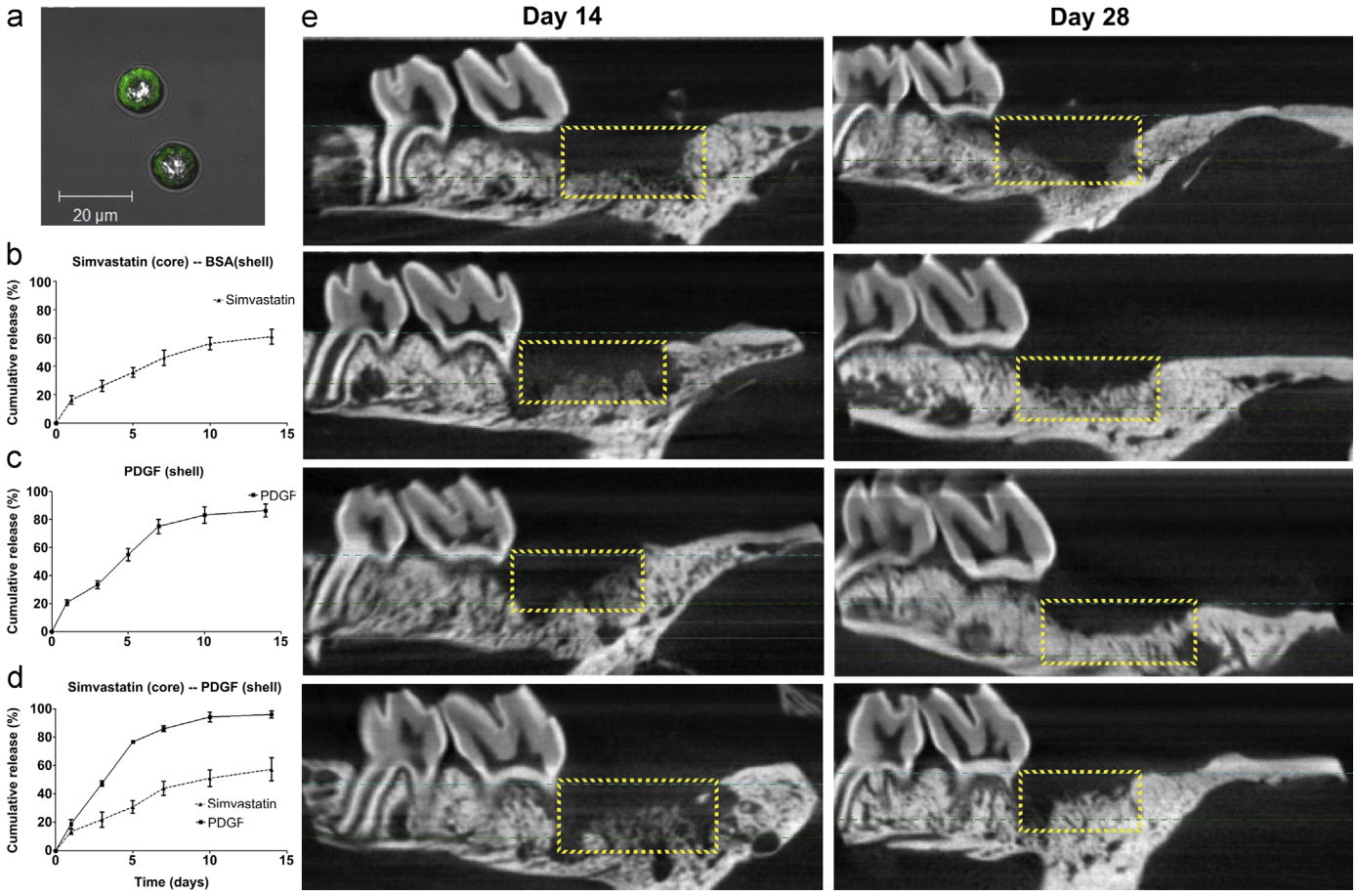


**Fig. 8.** (a) Fluorescent image illustrating core–shell structure of microspheres. (b–d) The in vitro release profiles of different formulations. (e) Micro-CT characterization of a sagittal slice crossing the mid-points of the maxillary second molar and third molar. BSA-BSA: BSA(core)–BSA(shell). (Reprinted from Chang et al., 2013, with permission from Elsevier.)

poly(vinyl alcohol) (PVA) hydrogel microspheres generated by submerged EHDA in conjunction with UV photopolymerization. The L929 fibroblasts that were loaded in PVA microspheres had viability more than 90% after culture for 24 h. Most recently, Gasperini et al. (2013) encapsulated B50 neuroblasoma rat cells in alginate beads by EHDA and found that the cells inside gel beads remained viable after encapsulation and maintained their ability to reattach and proliferate after being released. Zhang et al. (2013) developed a microcapsule with a diameter of 100 μm consisting of a liquid core and an alginate–chitosan–alginate shell by combining EHDA and layer-by-layer coating technique. The authors further examined the encapsulation and culture of embryonic stem cells in the liquid cores of these capsules. It was demonstrated the shell can greatly decrease immunoglobulin G binding to the loaded cells. Most importantly, Levit et al. (2013) demonstrated encapsulation of human mesenchymal stem cells (hMSCs) in alginate using EHDA and further incorporation of these cell-laden capsules in hydrogel. The gel loaded with microcapsules was employed as a patch for myocardial infarction repair in a rat model, showing the improvement of retention of hMSCs and cardiac function. In an earlier study, Goosen et al. (1997) demonstrated that somatic tissue encapsulated within alginate via EHDA could retain viability more than 2 months during culture. In a most recent study, Ma et al. (2013) demonstrated the encapsulation of rat pancreatic islets in the core of core–shell hydrogel microcapsules for the treatment of Type I diabetes using co-axial EHDA. This method could eliminate the issues of islet encapsulation such as insufficient immune-protection encountered by regular EHDA.

Owing to their sustained delivery properties, microparticles generated by EHDA show great potential for use in tissue regeneration. Chang et al. (2012) demonstrated the fabrication of microspheres encapsulating platelet-derived growth factor (PDGF) a mitogen and simvastatin a differentiation factor in the core and shell or vice versa presenting sequential and simultaneous release of PDGF and simvastatin for applications in periodontal regeneration. All microspheres showed adequate biocompatibility in vivo because of elevated proliferation, decreased apoptosis, and diminished inflammation. Their subsequent study further examined effects of the combination and sequential release of PDGF and simvastatin from core–shell microparticles encapsulating simvastatin in the core and PDGF in the shell on the periodontal regeneration (Chang et al., 2013). The microparticles had a diameter of around 15 μm with evident core-sheath structure, which released PDGF rapidly followed by gradual-release of simvastatin, showing significantly larger volume fraction of regenerated bone tissue and a clear reduction in trabecular separation at day 14 and 28 when compared to the control (Fig. 8). Their most recent study showed that microparticles with sequential release of PDGF and simvastatin could accelerate the dentoalveolar regeneration by enhancing osteoblastogensis and promoting bone maturation (Chang et al., 2014). In a separate study, Guo et al. (2014) fabricated PLA–PEG microparticles with the loading of calcium phosphate-pDNA nanoparticles via electrospray. They found that subcutaneous infusion of microparticles with encapsulated both calcium phosphate–pVEGF and calcium phosphate–pbFGF nanoparticles can significantly increase the densities of blood vessels and induce a rapid maturation of blood vessels with marginal probability of cytotoxicity and inflammatory response.

Due to the surface charges carried by electrosprayed particles, they can be easily deposited on the conductive substrate during

the EHDA process. Lee et al. (2010a) demonstrated the coating of basic fibroblast growth factor (bFGF) loaded PLGA nanoparticles to anodized titanium implants by EHDA. The results showed that the coating PLGA incorporated with bFGF to a titanium implant could enhance bone formation near the surface of an implant inserted in bone. The mean bone-to-implant contact percentage was significantly greater for the implant (44.7%) coated with PLGA/bFGF nanoparticles (100 ng bFGF) comparing to other implants (31.4% and 33.6%) tested. Cho et al. (2011) demonstrated the surfaces coated with 1,25-dihydroxyvitamin $D_3$-loaded PLGA particles via electrospray can promote osseointegration of anodized titanium implants. Shim et al. (2013) showed anodized Ti discs partially coated with fibroblast growth factor-2 (FGF-2)-loaded PLGA nanoparticles by electrospray deposition. The coating retained their original porous structure and simultaneously exhibited a continuous release of FGF-2 for 2 weeks. The implants were tested in a rabbit tibia model, indicating the mean osseointegration for coated implants was much higher (70.1%) than that of bare implants (47.1%). EHDA has also been used to pattern nano-hydroxyapatite and silicon-doped nano-hydroxyapatite on the titanium surface, providing a way for modifying the surfaces of implants to regulate and direct cellular behaviors for tissue regeneration (Li et al., 2008; Munir et al., 2011). These studies suggest that electrospray deposition is a facile method for coating medical devices to maintain their surface topography and simultaneously delivering growth factors in a sustained manner for promoting bone regeneration.

EHDA can also combine with electrospinning to create functional scaffolds and tissue constructs for tissue regeneration. Francis et al. (2010) demonstrated that electrospraying nano-hydroxyapatite to electrospun polymeric nanofiber scaffolds could be a promising approach for the fabrication of composite nanofibrous scaffolds in bone tissue regeneration. Stankus et al. (2007) fabricated cell microintegrated blood vessel constructs by electrospraying smooth muscle cells synchronously with electrospinning of poly(ester urethane) urea (PEUU) a biodegradable elastomer, representing a typical engineering approach for replacing blood vessels. Tang et al. (2013) developed a technique combining electrospray and electrospinning for preparing fiber-microsphere scaffolds that could incorporate bioactive molecules in a gradient fashion. Such scaffolds could be used for interface tissue engineering. More recently, Bock et al. (2014) demonstrated that the direct electrospraying of microparticles with encapsulation of a model protein on highly melt electrospun fiber scaffolds could achieve a duplicable coating throughout the whole construct. The scaffolds showed a positive effect when culturing with preosteoblast cells for 18 days. This design could be promising for growth factor delivery during tissue regeneration. The following studies additionally showed the potential of EHDA for applications in tissue engineering. Martyn et al. (2011) demonstrated the deposited fibronectin by electrospray retains the ability to promote cell adhesion. Li et al. (2010) generated both continuous and discrete density gradients composed of biodegradable polymeric microparticles using electrospray deposition. The developed substrates with gradients in microparticle density have potential applications in neural tissue engineering.

### 9.5. Sensing

Metal oxides have been used as sensing materials for various types of gases due to their simplicity, small dimensions and low cost. Matsushima et al. (2004) prepared the films composed of multiple layers of $SnO_2$ particles on the glass substrates utilizing the electrospray pyrolysis approach. The particles showed sensing properties for $H_2$. Cusano et al. (2006) demonstrated the $SnO_2$ layer deposition on the silica optical fiber via electrospray pyrolysis for the detection of sub-ppm ammonia concentrations in water environments. The results of room temperature adsorption experiments revealed the high sensor resolution of 80 ppb, good recovery characteristics, high repeatability and short response time. Metal oxides including Cu-doped $SnO_2$, $WO_3$, and $In_2O_3$ thin films were also fabricated using electrospray deposition for sensitive and selective detection of hydrogen sulfide (Materi et al., 2007, 2009; Ghimbeu et al., 2007, 2009). It was shown that Cu–$SnO_2$ films could readily detect very low concentrations of $H_2S$ when the operating temperatures were 100 and 200 °C. Gaury et al. (2013) prepared Nb-doped $WO_3$ thin films by electrospraying a tungsten isopropoxide in 2-propanol precursor solution on glass substrates for potential use in gas sensors. In a different study, Lee (2013) fabricated polypyrrole/iron oxyhydroxide hybrid nanoparticles using co-axial electrospray and heat stirring process for nerve gas sensing applications. Their most recent study demonstrated the production of urchin-like polypyrrole nanoparticles with various diameters using co-axial electrospray and vapor deposition polymerization (Lee et al., 2014). It was demonstrated that urchin-like particle-based sensors had greater sensitivity and ca. 10–100 times higher minimum detectable levels of common analytes than pristine polypyrrole particle-based sensors.

## 10. Scale up

There are several commercially available electrospray aerosol generators (e.g. TSI Model 3480 and Ioner Electrospray ES-3020), which are a single-capillary electrospray system similar to the setup in most of the laboratories. The particle generation rate is around $10^7$ particles per $cm^3$. Mass production can be simply achieved by increasing flow rate of the spraying solution. However, the particle size increases with increasing flow rate based on the scaling laws. Alternatively, operating a number of Taylor cones in parallel can increase the throughput in electrospray while maintaining the particle size. Rulison and Flagan (1993) firstly reported a linear array of capillary electrodes opposite a slotted flat plate counter-electrode, providing a means of greatly increasing the production rate in electrospray. Almekinders and Jones (1999) then showed an injector with 24 electrospray emitters equidistantly arranged on a straight line 15 cm long for enhancing production rate. EHDA scaling up study for a four capillary array conducted by Regele et al. (2002) showed that the required potential for the production of uniform sized particles in stable Taylor cone–jet conditions is a function of distance between two neighboring nozzles. Their results also represented that the electric potential required for the formation of stable Taylor cone–jet increases as the capillary spacing decreases and vice versa. However, in an extremely close nozzles' configuration, the required electric potential decreases due to the cumulative effects of electric fields in axial direction. Bocanegra et al. (2005) developed an electrospray atomizer having 37 holes and 115 emitters per $cm^2$ for increasing the liquid flow rates (Fig. 9), demonstrating simple orifices rather than needles were suitable for atomizing liquids in steady cone–jet mode. Subsequently, Deng (2006, 2007) developed a system consisting of a microfabricated liquid distributor having multiple electrospray sources in order to increase the throughput. The scale-up electrospray system has been applied in agriculture, sanitation and other industrial applications (ESS Electrostatic Spray System, Inc.).

## 11. Modeling and simulation

In the process of electrohydrodynamic atomization, the formation stable Taylor cone–jet as well as the mechanism of

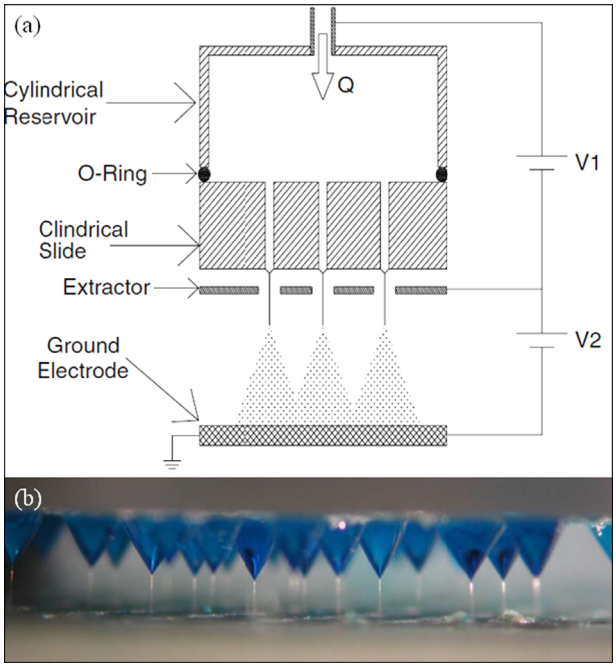


**Fig. 9.** A sketch of multi-hole EHDA (a); a real multi-hole EHDA process (b) (reprinted from Bocanegra et al., 2005, with permission from Elsevier). (For interpretation of the references to color in this figure legend, the reader is referred to the web version of this article.)

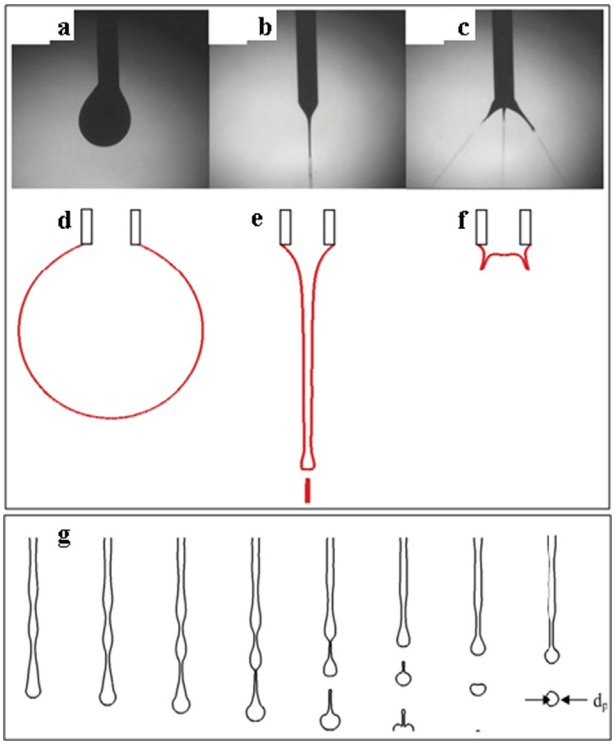


**Fig. 10.** Comparison between experimental (a–c) and simulation (d–f) results of DCM electrospray; Wave-like structure of unstable jet and formation of micro droplet (g) (reprinted from Lim et al., 2011. Copyright 2011 John Wiley & Sons, Inc.). (For interpretation of the references to color in this figure legend, the reader is referred to the web version of this article.)

electrosprayed particle transport, solvent evaporation, and collection or deposition are critical stages for large scale production of uniform sized micro/nano particles. In order to provide a deeper understanding EHDA behavior, several studies have been conducted to model or simulate each of aforementioned mechanisms.

### 11.1. Simulation of EHDA

One of the basic issues in EHDA modeling is the mechanism of electric charge transport in liquid phase, which is used to evaluate the electrical stress exerted on the free surface of the liquid. Overall, we may consider three different charge transport models known as (1) perfect conductor model, (2) perfect dielectric, and (3) leaky dielectric model. In perfect conductors such as liquid metals, it is assumed that the electric charges are localized at the liquid–gas interface, and consequently no electric field exists inside the liquid. It means the charge relaxation time, which is defined as electrical permittivity to electrical conductivity ratio ($\tau^E = \varepsilon/K$), is significantly shorter than viscous flow ($\tau^v \sim \rho L^2/\mu$) and surface tension ($\tau^\gamma \sim \sqrt{\rho L^3/\gamma}$) time scales. In a perfect dielectric liquid (e.g. highly pure heptane), no electric fields exist both inside and at the liquid–gas interface. Therefore, the effect of external electric field is confined to electrical polarization stress at the liquid surface. However, when the charge relaxation time is in the same order of magnitude of viscous flow and surface tension tame scales, neither the aforementioned conditions can properly describe charge transport within the system. Therefore, a leaky dielectric model has been proposed to overcome such confinement.

Till now, to predict the behavior of a liquid flow inside and outside the Taylor conical meniscus and to describe the breakup of a stable jet into charged drops in EHDA process, several scaling laws and modeling and simulation studies have been reported. However, most of them considered the Taylor cone and the jet extending from the conical tip as two separate processes. In 1994, Shtern and Barrero (1994) adopted the liquid circulation behavior inside the Taylor-cone to a simplified model based on exact solution of Navier–Stokes equations. The stability of the emitted jet was studied either as a charged jet in the absence of the electric field (Basset, 1989; Taylor, 1969; Saville, 1971b) and an uncharged jet in the presence of electric field (Nayyar and Murty, 1960; Saville, 1970, 1971a). However, due to co-existence of both charged jet and electric field in actual EHDA process, the interactions of surface charges and external electric field in a leaky dielectric condition was investigated by Mestel (1994). Despite valuable theoretical studies on Taylor cone and jet separately, the complicated nature of Taylor cone–jet mechanism has confined comprehensive studies for understanding the actual mechanism behind the Taylor cone–jet behavior.

In 2003, Yan et al. (2003) presented a computational fluid dynamics (CFD) based model for 2D axi-symmetric simulation of cone–jet formation for electrosprayed ethylene glycol and 1-octanol meniscus. The indicated model was able to compute the formation of cone and jet as well as the velocity and electric field inside the cone–jet. However, despite a good consistency with the experimental results, the model failed to predict the droplet formation following the jet breaking up. Lastow and Balachandran (2006) employed the commercial software package CFX 4.4 to develop a 2D axi-symmetric model via solving Navier–Stokes equations at the presence of electric field, but without considering the electrical current in the system. Although the model did not predict the droplet formation, the size of the ethanol droplet calculated from jet diameter compared well with the experimental observations.

Recently, by considering the front tracking/finite volume method proposed by Hua and Lou (2007) and Lim et al. (2010) developed a CFD code, to numerically investigate a single liquid cone–jet as well as the formation of droplet. They solved a full set of Navier–Stokes equations for the liquid and gas (air) phases, where the liquid–gas interface was monitored by a front tracking approach. The simulation results were found to compare well with experiments (Fig. 10a–f).

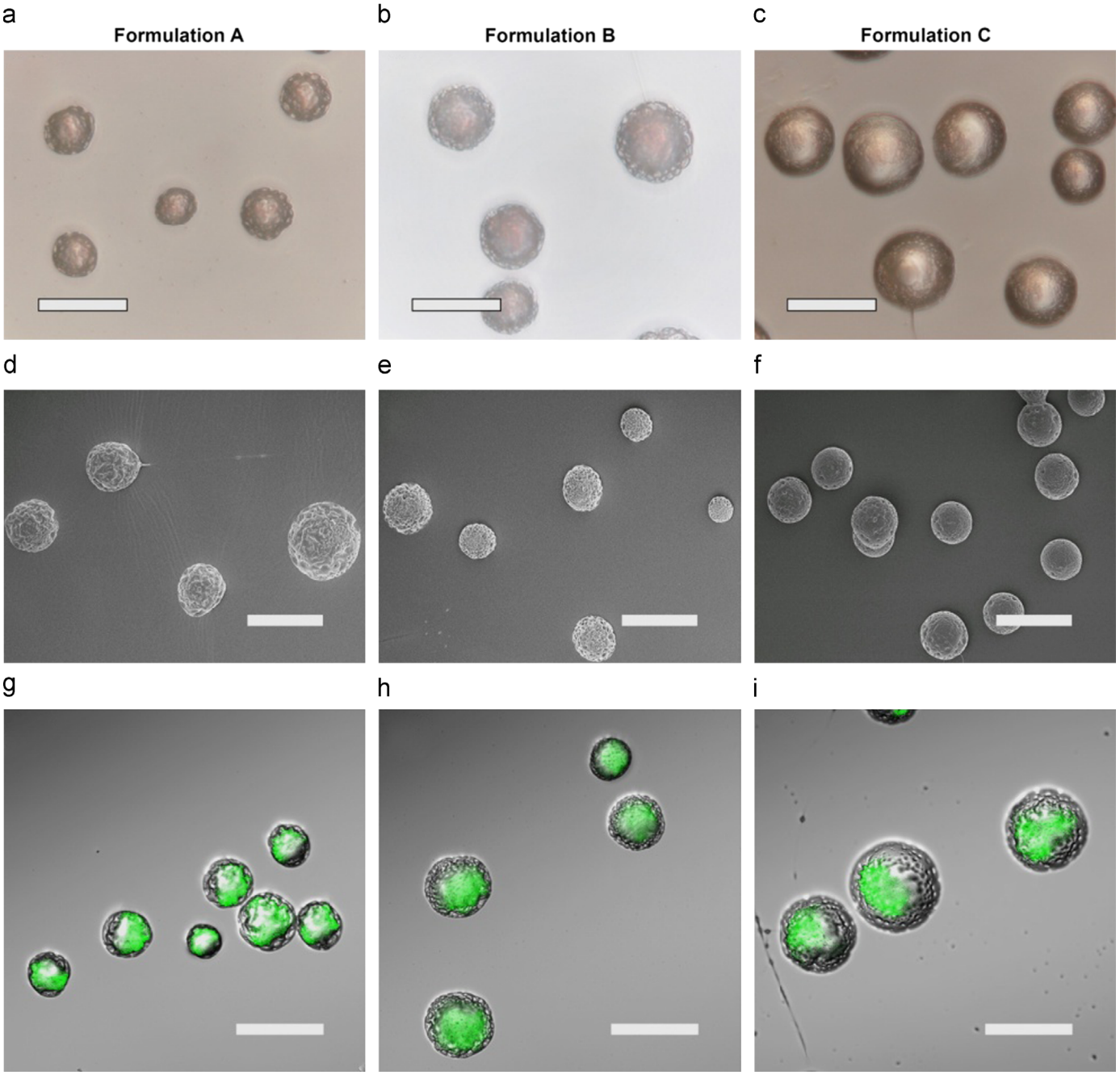


**Fig. 11.** Transmitted light microscopy (a–c), scanning electron microscopy (SEM) (d–f), and laser confocal scanning microscopy (g–f) of core–shell microparticles produced using coaxial electrohydrodynamic atomization The green light represent the location of core structure (PLGA) surrounded by shell (PDLLA) (reprinted from Xu et al., 2013a, with permission from Elsevier). (For interpretation of the references to color in this figure legend, the reader is referred to the web version of this article.)

Their CFD simulation results also revealed that the droplet formation at end of the jet stream is due to the wave like structure on the jet surface resulting from surface tension forces (Fig. 10g). These results compared well with Hohman et al.'s (2001) experimental observations on the unstable jet structure.

### *11.2. Simulation of co-axial electrohydrodynamic process*

For the preparation of core–shell microparticles, Xu et al. (2013a) applied a strong electric field between a co-axial capillary nozzle and a grounded substrate. Polymeric composite double-layered microparticles with poly ($_{D,L}$-lactic acid) (PDLLA) shell surrounding a PLGA core were produced successfully in a stable Taylor cone–jet conditions (Fig. 11).

For the simulation of the process, they employed a commercial CFD software, FLUENT 14.0 (ANSYS, Inc; Canonsburg, PA), to solve Navier–Stokes equation, including surface tension and electrical stress exerted by an external electric field on the liquid–gas interface. Since the presence of charged liquid does not affect the electric potential far from the nozzle, they first determined electric potential in a large domain including the co-axial nozzle and the collecting substrate. Next, the electric potential value was extracted and imposed to a smaller domain near the nozzle as boundary conditions. Their results demonstrated that there are two significant liquid vortexes located near the shell channel outlet and below the cone surface (Fig. 12). However, the liquid placed near the liquid–gas interface is pushed toward the jet stream by external electric forces. Therefore, to form droplets

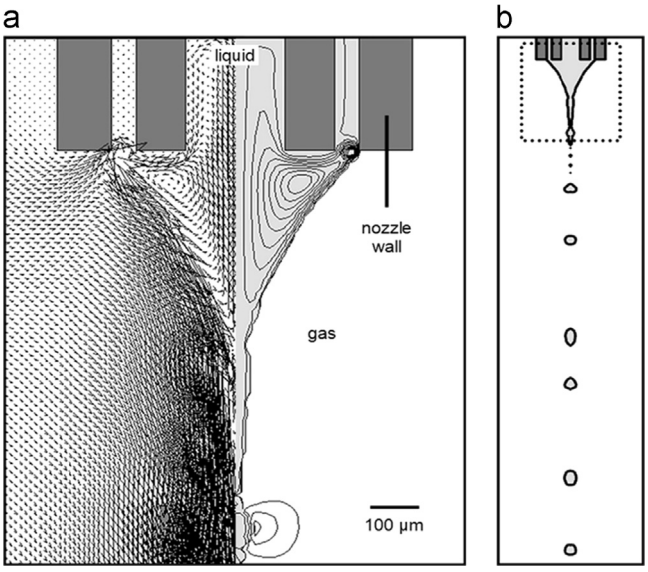


**Fig. 12.** The streamline and velocity field within a stable liquid cone–jet (a). This system was used for fabrication of core–shell microparticle. The location of plotted region and the CFD domain (b). For simulation of EHDA and co-axial EHDA system, first, the electric field strength was calculated for the whole setup. Then the electric field was extracted and applied to the CFD domain as boundary conditions (reprinted from Xu et al., 2013a, with permission from Elsevier).

comprised core and shell fluids, the nozzle voltage must be sufficiently high to pull the core fluid toward the interface and into the jet stream.

*11.2.1. Governing equations*

For the simulation of EHDA process, the governing equations (e.g. mass conservation and Navier–Stokes equations) regarding the motion of liquid(s) and gas phases must be solved, where the fluids are assumed to be incompressible.

$$\nabla \cdot \mathbf{u} = 0 \tag{16}$$

$$\rho\frac{\partial \mathbf{u}}{\partial t} + \rho\mathbf{u}\cdot\nabla\mathbf{u} = -\nabla P + \mu\,\nabla^2\mathbf{u} + \mathbf{F}_{ES} + \mathbf{F}_{ST} + \left(\rho - \rho_g\right)\mathbf{g} \tag{17}$$

In Eqs. (16) and (17), $\rho$ and $\rho_g$ are the density of liquid(s) and gas phases, $\mathbf{u}$ is the velocity of the fluid, $P$ is the pressure of the fluid (s), $\mu$ viscosity of the fluid(s) and $\mathbf{g}$ is the gravitational acceleration. $\mathbf{F}_{ES}$ and $\mathbf{F}_{ST}$ are the electric field stresses exerted on the liquid–gas free interface by an external electric field and surface tension, respectively. $\mathbf{F}_{ES}$ can be calculated from the divergence of the Maxwell stress tensor as follows:

$$\mathbf{F}_{ES} = \nabla\sigma^M = q_v\mathbf{E} - \tfrac{1}{2}E^2\nabla\varepsilon \tag{18}$$

where $q_v$ is the volume charge density at the interface, $\mathbf{E}$ is the electric field near the interface, and $\varepsilon$ is the electrical permittivity of the liquid.

This equation comprises the Coulombic force due to interaction of the electric charges with the external electric field at the interface (the first term on the right) and polarization stress acting in normal direction of interface (the second term on the right). The surface tension acting on the liquid–gas interface as a volume force is defined by Eq. (19), which is the function of surface curvature ($\kappa$), surface normal vector ($n = \nabla\alpha_i$) and the volume fraction of the $i$th phase.

$$\boldsymbol{F}_{ST} = \sum_{ij,i<j}\gamma_{ij}\frac{\alpha_i\rho_i\kappa_j\nabla\alpha_j + \alpha_j\rho_j\kappa_i\nabla\alpha_i}{(1/2)(\rho_i+\rho_j)} \tag{19}$$

If the above formula is applied for the two phases exist in a computational cells, it is simplified to the following expression:

$$\boldsymbol{F}_{ST} = \gamma_{ij}\frac{\rho\kappa_i\nabla\alpha_i}{(1/2)(\rho_i+\rho_j)} \tag{20}$$

where $\rho$ is the volume average density.

In order to define electric potential, Poisson's equation (Eq. (21)) must be solved. Subsequently, the electric field vector (Eq. (22)) is calculated as negative gradient of the electric potential.

$$-\nabla\cdot\left(\varepsilon_0\nabla\phi\right) = q_v \tag{21}$$

$$\mathbf{E} = -\nabla\phi \tag{22}$$

In the simulation of multi-phase problems, particularly EHDA, tracking liquid–liquid (for co-axial EHDA) and liquid–gas interfaces are challenging issues. In the literature, there are several techniques proposed for explicitly or implicitly tracking the interface of two immiscible fluids (Slavov and Dimova, 2007). The former includes boundary integral method, front tracking method, and immersed interface techniques. However, the latter includes the volume of fluid (VOF), the phase-field method, the Lattice–Boltzmann method, and the level set method. Both demonstrated categories can handle the complicated interface deformation successfully (Liu and Nguyen, 2010).

In 2010, Lim et al. (2010) applied the front tracking method for simulating a single nozzle EHDA, where the interface had a thickness of the same order of magnitude as computational cells. They assumed that the physical properties varied smoothly and continuously from the first phase to the second one, which can be described by a field distribution function as follows:

$$b(\mathbf{x},t) = b_g + \left(b_l - b_g\right)\cdot\mathbf{I}(\mathbf{x},t) \tag{23}$$

where $b_l$ and $b_g$ are the physical properties of liquid and gas phases, respectively.

$\mathbf{I}(\mathbf{x},t)$ is an indicator function with values one and zero for liquid and gas phases, respectively, which is defined over the inner domain $\Omega$ surrounded by the interface. In the indicator function, $\delta(\mathbf{x}-\mathbf{x}_f)$ represents a delta function.

$$\mathbf{I}(\mathbf{x},t) = \int_{\Omega}\delta(\mathbf{x}-\mathbf{x}_f)\,d\vartheta_f \tag{24}$$

The same group (Xu et al., 2013a) applied the VOF model for tracking the interface deformation during Taylor cone–jet formation. They used the volume fraction function (Eq. (25)) to find the interface location lies within computational cells. For these cells $\alpha$ varies from 0 to 1 (Hirt and Nichols, 1981). Thus, the volume fraction function of unity means that whole cell is filled with the primary (e.g. liquid) phase and vice versa.

$$\frac{\partial\alpha_i}{\partial t} + \nabla\cdot(\alpha_i\boldsymbol{u}_i) = 0 \tag{25}$$

To solve this equation, the initial approximation for the interface location has to be provided. After solving the equation, the interface should be reconstructed to calculate the weighted density and viscosity for computational sub-domains, and subsequently to calculate the volume flux of the convective parameters in the governing equations (Hirt and Nichols, 1981).

*11.3. Deposition and collection*

As presented in Section 8, compared to traditional deposition, printing, and micro-patterning techniques such as photolithography, soft lithography, and ink jetting, electrospray deposition is a simple, in-expensive, and readily adjustable and robust technique for micro-patterning, particularly for biodegradable microparticle depositions (Rezvanpour and Wang, 2011).

Since numerical simulation is an indispensable tool for the optimization of deposition pattern, besides experimental investigations, researchers have developed numerical models to describe the charged droplets transport and spatial particle distribution in the presence of an imposed electric field and to predict the electrosprayed micro-pattern deposition. Ganan-Calvo et al. (1994) and Hartman et al. (1999) described the transport of droplets generated by EHDA through a numerical modeling approach. Wihelm et al. (2003) developed a numerical study to describe the reason behind the variations in the thickness of the layer constructed by deposited particles on the surface of the substrate. In 2011, Rezvanpour and Wang (2011) investigated the deposition of microparticles on a substrate covered by a metallic mask and proposed a numerical simulation for conditions where an additional electric potential source is applied to the mask. Their experimental and computational results showed a well-focused micro-pattern on the surface of the substrate.

*11.3.1. Governing equations for EHDA deposition*

The equation of motion of the falling spherical charged particles was developed via force balance under the effect of an external electric field as follows (Crowe et al., 1995; Yang et al., 1993; Jung et al., 2010; Rezvanpour and Wang, 2014):

$$m_p \frac{d\mathbf{u}_p}{dt} = \sum \mathbf{F} = \mathbf{F}_E + \mathbf{F}_q + \mathbf{F}_D + \mathbf{F}_g + \mathbf{F}_B \tag{26}$$

where $m_p$, $\mathbf{u}_p$, $\mathbf{F}_E$, $\mathbf{F}_q$, $\mathbf{F}_D$, $\mathbf{F}_g$, and $\mathbf{F}_B$ represent particle mass, particle velocity vector, electric force imposed on the surface of the particles by an external electric field, Coulombic repulsive force, drag force exerted by the surrounding gas, gravitational force, and other body forces, respectively. The body forces include buoyancy force and image force, which is due to the electric force between charged particles and the induced charges on the surface of a conductive collector. The details of the closures for aforementioned forces in the modeling of the charged particle deposition can be found in the literature (Jung et al., 2010; Sigmond, 1982; Xie et al., 2010) and are not reproduced here for brevity of presentation.

## 12. Concluding remarks and perspectives

EHDA offers a facile and robust method of producing particles with well-controlled size, morphology, structure, and shapes for various applications. EHDA also offers an approach for processing fine particles including charging, dispersing, coating and deposition. Although substantial progress has been achieved, additional efforts are still needed in the development and applications of EHDA on the fabrication and processing of particulate materials. For example, while particles with sizes in tens of nanometers have been achieved, the flow rates used in those studies are usually very low, resulting in a very low production rates. Devices and technologies should be further developed to enhance production rate, in particular, for the fabrication of particles less than 100 nm.

EHDA has been demonstrated for the production of core–shell particles. The particles with core–shell structure hold great potential for sequential release of antiangiogenetic agents and anticancer drugs, which may be more effective to treat tumors as the antiangiogenetic agents can first block the nutrition transport to the tumor and then anticancer drugs can kill the tumor cells (Sengupta et al., 2005). By incorporating radiosensitizing agent, chemotherapeutic agent, and photothermal agent or nanostructured materials, electrosprayed particles can combine different therapies including radiation therapy, chemotherapy, and photothermal therapy for combating cancer. It seems that EHDA has no limitation in terms of materials. More efforts may be placed on the use of smart materials for drug delivery including pH-responsive materials, temperature-sensitive materials, and enzyme-responsive materials. At the same time, chemistry can be used to modify the raw materials or the surface of particles produced by EHDA with targeting moieties for targeted drug delivery, which may eliminate the side effects of drugs to a greater extent. Though EHDA has been demonstrated to simultaneously encapsulate multiple contrast agents and drugs in particles, future studies may put more efforts on the use of EHDA for the development of multifunctional particles capable of diagnosis, targeted drug delivery, and monitoring of therapeutic response. Although many particulate formulations based on electrosprayed particles have been developed, their efficacy for drug delivery have not been thoroughly validated in animal models not even to say in clinical trials. Future work should also involve more collaborative efforts to test the efficacy of these particulate formulations between multidisciplinary experts including engineers, chemists, material scientists, and clinicians.

In addition, particles generated by EHDA have been demonstrated for use in tissue regeneration. Future studies may consider the encapsulation of contrast agents in the particles for better monitoring the tissue regeneration process using imaging modalities. Future studies may also consider the generation of electrosprayed particles with encapsulation of multiple growth factors or signaling molecules that can precisely control the release of these molecules in specific temporal and spatial patterns closely mimicking tissue development for better tissue regeneration. The particles generated by EHDA can be incorporated into traditional tissue engineering matrices (e.g. hydrogels and sponges) for tissue regeneration. Particles generated by EHDA carry charges on the surface during fabrication. Electrical field has been used to guide the trajectory of particles, which could help the fabrication of 3D scaffolds using particles as building blocks. Alternatively, magnetic nanoparticles can be encapsulated in microparticles generated by electrospray that can be assembled into a desired structure by applying a magnetic field. EHDA in the dripping mode could be capable of producing monodispersed microparticles with highly porous structure. These particles could be used as cell carriers providing a noninvasive means for cell delivery through direct injection of cell-seeded microparticles to the injured sites unlike surgical implantation. Cells/tissues can be encapsulated in the hydrogel microbeads using EHDA in the dripping mode. These cell/tissue-laden microbeads hold great promise in drug delivery (e.g. insulin secretion and endostatin secretion) and tissue regeneration (Jacobs-Tulleneers-Thevissen et al., 2013; Joki et al., 2001; Kachouie et al., 2010). In addition, cells after electrospray can maintain their proliferation and function. Therefore, electrohydrodynamic jet printing can be used to pattern bioactive molecules and cells on various surfaces of different types of substrates including electrospun nanofiber scaffolds. The bioactive molecule and cell patterning could be used to create desired tissue architecture for regenerating and repairing damaged tissues. EHDA may contribute to the improvement of other technologies in terms of their capabilities. For example, electrospraying nozzle combining with 3D printer could improve the resolution of current 3D printing systems.

## Acknowledgments

This work was supported partially from startup funds from University of Nebraska Medical Center and National Institute of General Medical Science (NIGMS) Grant 2P20 GM103480-06. C.H.W. acknowledges the funding support from the National Medical Research Council (NMRC, Singapore) under the Grant no. NMRC EDG11may084.

## Appendix A. Supporting information

Supplementary data associated with this article can be found in the online version at: http://dx.doi.org/10.1016/j.ces.2014.08.061.

## References


Abeyewickreme, A., et al., 2009. Bio-electrospraying embryonic stem cells: interrogating cellular viability and pluripotency. Integr. Biol. 1 (3), 260–266.

Ahmad, Z., et al., 2010. Electrohydrodynamic direct writing of biomedical polymers and composites. Mater. Eng. 295 (4), 315–319.

Almekinders, J.C., Jones, C., 1999. Multiple jet electrohydrodynamic spraying and applications. J. Aerosol Sci. 30 (7), 969–971.

Almeria, B., et al., 2010. Controlling the morphology of electrospray-generated PLGA microparticles for drug delivery. J. Colloid Interface Sci. 343 (1), 125–133.

Almeria, B., Gomez, A., 2014. Electrospray synthesis of monodisperse polymer particles in a broad (60 nm–2 μm) diameter range: guiding principles and formulation recipes. J. Colloid Interface Sci. 417 (1), 121–130.

Ambrus, et al., 2013. Analysis of submicron-sized niflumic acid crystals prepared by electrospray crystallization. J. Pharm. Biomed. Anal. 76, 1–7.

Anthony, D., et al., 2014. Scalable, semicontinuous production of micelles encapsulating nanoparticles via electrospray. Langmuir 30 (4), 3939–3948.

Anumolu, R., et al., 2011. Fabrication of highly uniform nanoparticles from recombinant silk–elastin-like protein polymers for therapeutic agent delivery. ACS Nano 5 (7), 5374–5382.

Arya, N., et al., 2009. Electrospraying: a facile technique for synthesis of chitosan-based micro/nanospheres for drug delivery applications. J. Biomed. Mater. Res. Part B: Appl. Biomater. 88B (1), 17–31.

Avseenko, N.V., et al., 2001. Immobilization of proteins in immunochemical microarrays fabricated by electrospray deposition. Anal. Chem. 73 (24), 6047–6052.

Avseenko, N.V., et al., 2002. Immunoassay with multicomponent protein microarrays fabricated by electrospray deposition. Anal. Chem. 74 (5), 927–933.

Bai, M., Liu, S.Z., 2014. A simple and general method for preparing antibody–PEG–PLGA sub-micron particles using electrospray technique: an in vitro study of targeted delivery of cisplatin to ovarian cancer cells. Colloids Surf. B Biointerfaces 117C (1), 346–353.

Barrero, A., 2007. Micro- and nanoparticles via capillary flows. Annu. Rev. Fluid Mech. 39 (1), 89–106.

Basset, A.B., 1989. Waves and jet in a viscous liquid. Am. J. Math. 16 (1), 93–110.

Berkland, C., et al., 2004. Controlling surface nano-structure using flow-limited field-injection electrostatic spraying (FFESS) of poly(d,L-lactide-co-glycolide). Biomaterials 25 (25), 5649–5658.

Bhaskar, S., et al., 2008. Spatioselective modification of bicompartmental polymer particles and fibers via huisgen 1,3-dipolar cycloaddition. Macromol. Rapid Commun. 29 (24), 1655–1660.

Bhaskar, S., et al., 2010. Towards designer microparticles: simultaneous control of anisotropy, shape, and size. Small 6 (3), 404–411.

Bocanegra, R., et al., 2005. Multiple electrosprays emitted from an array of holes. J. Aerosol Sci. 36 (12), 1387–1399.

Bock, N., et al., 2011. Electrospraying, a reproducible method for production of polymeric microspheres for biomedical applications. Polymer 3 (1), 131–149.

Bock, N., et al., 2012. Electrospraying of polymers with therapeutic molecules: state of the art. Prog. Polym. Sci. 37 (11), 1510–1551.

Bock, N., et al., 2014. Composites for delivery of therapeutics: combining melt electrospun scaffolds with loaded electrosprayed microparticles. Macromol. Biosci. 14 (2), 202–214.

Bodnar, E., Rosell-Liompart, J., 2013. Growth dynamics of granular films produced by electrospray. J. Colloid Interface Sci. 407 (1), 536–545.

Bohr, A., et al., 2012. Release profile and characteristics of electrosprayed particles for oral delivery of a practically insoluble drug. J. R. Soc. Interface 9 (75), 2437–2449.

Borra, J.P., et al., 1999a. Bipolar coagulation for powder production: micro-mixing inside droplets. J. Aerosol Sci. 30 (7), 945–958.

Borra, J.P., et al., 1999b. Influence of electric field profile and polarity on the mode of EHDA related to electric discharge regimes. J. Aerosol Sci. 30 (7), 913–925.

Braghirolli, D.I., et al., 2013. Bio-electrospraying of human mesenchymal stem cells: an alternative for tissue engineering. Biomicrofluidics 7 (4), 044130.

Camelot, D.M.A., et al., 1999. Experimental study of the jet break up for ehda of liquids in the cone-jet mode. J. Aerosol Sci. 30 (7), 976–977.

Cao, L., et al., 2014. Generation of nano-sized core–shell particles using a coaxial tri-capillary electrospray-template removal method. Colloids Surf. B: Biointerfaces 115 (1), 212–218.

Chang, M., et al., 2010a. A new method for the preparation of monoporous hollow microspheres. Langmuir 26 (7), 5115–5121.

Chang, M., et al., 2010b. Controlling the thickness of hollow polymeric microspheres prepared by electrohydrodynamic atomization. J. R. Soc. Interface 7 (Suppl. 4), S451–S460.

Chang, P., et al., 2012. Biocompatibility of PDGF-simvastatin double-walled PLGA (PDLLA) microspheres for dentoalveolar regeneration: a preliminary study. J. Biomed. Mater. Res. A 100A (11), 2970–2978.

Chang, P., et al., 2013. Dual delivery of PDGF and simvastatin to accelerate periodontal regeneration in vivo. Biomaterials 34 (38), 9990–9997.

Chang, P., et al., 2014. Sequential platelet-derived growth factor—simvastatin release promotes dentoalveolar regeneration. Tissue Eng. Part A 20 (1–2), 356–364.

Chen, C.H., et al., 2006. Electrohydrodynamic "drop-and-place" particle deployment. Appl. Phys. Lett. 88, 154104.

Chen, D.R., Pui, Y.H., 1997. Experimental investigation of scaling laws for electrospraying: dielectric constant effect. Aerosol Sci. Technol. 27 (3), 367–380.

Chen, D.R., et al., 2000. A novel approach for introducing bio-materials into cells. J. Nanopart. Res. 2 (2), 133–139.

Chen, H., et al., 2008. One-step multicomponent encapsulation by compound-fluidic electrospray. J. Am. Chem. Soc. 130 (25), 7800–7801.

Clarke, J.D., Jayasinghe, S.N., 2008. Bio-electrosprayed multicellular zebrafish embryos are viable and develop normally. Biomed. Mater. 3 (1), 011001.

Cho, Y., et al., 2011. Promotion of osseointegration of anodized titanium implants with a 1α, 25-dihydroxyvitamin d3 submicron particle coating. Int. J. Oral Maxillofac. Implant. 26 (6), 1225–1232.

Choi, J.S., et al., 2013. Electrospun chitosan microspheres for complete encapsulation of anionic proteins: controlling particle size and encapsulation efficiency. AAPS PharmSciTech 14 (2), 794–801.

Coll, A., et al., 2013. Colloidal crystals by electrospraying polystyrene nanofluids. Nanoscale Res. Lett. 8, 26.

Cooley, J.F., 1900. Improved methods of and apparatus for electrically separating the relatively volatile liquid component from the component of relatively fixed substances of composite fluids. Patent GB 06385.

Croisier, F., Jerome, C., 2013. Chitosan-based biomaterials for tissue engineering. Eur. Polym. J. 49 (4), 780–792.

Crowe, C.T., et al., 1995. A turbulent flow without particle mixing. Aerosol Sci. Technol. 22 (1), 135–138.

Cusano, et al., 2006. Nanowire photonic crystal waveguides for single-atom trapping and strong light–matter interactions. Appl. Phys. Lett. 104 (11), 111103.

Davies, L.A., et al., 2005. Electrohydrodynamic comminution: a novel technique for the aerosolisation of plasmid DNA. Pharm. Res. 22 (8), 1294–1304.

De La Mora, J.F., Loscertales, I.G., 1994. The current emitted by highly conducting Taylor cones. J. Fluid Mech. 260, 155–184.

Deng, W., 2007. Influence of space charge on the scale-up of multiplexed electrosprays. J. Aerosol Sci. 38 (10), 1062–1078.

Deng, W., et al., 2006. Increase of electrospray throughput using multiplexed microfabricated sources for the generation of monodisperse droplets. J. Aerosol Sci. 37 (6), 696–714.

Deotare, P.B., Kameoka, J., 2006. Fabrication of silica nanocomposite-cups using electrospraying. Nanotechnology 17 (5), 1380–1383.

Ding, L., et al., 2005. Fabrication of monodispersed taxol-loaded particles using electrohydrodynamic atomization. J. Control. Rel. 102 (2), 395–413.

Doi, T., et al., 2009. Single-step synthesis of nanosized titanium-based oxide/carbon nanotube composites by electrospray deposition and their electrochemical properties. J. Phys. Chem. C 113 (18), 7719–7722.

Doshi, N., et al., 2009. Red blood cell-mimicking synthetic biomaterial particles. Proc. Natl. Acad. Sci. USA 106 (51), 21495–21499.

Drozin, V.G., 1955. The electrical dispersion of liquids as aerosols. J. Colloid Sci. 10, 158–164.

Du, Y., et al., 2011. Fabrication, magnetic, and ferroelectric properties of multiferroic $BiFeO_3$ hollow nanoparticles. J. Appl. Phys. 109 (7), 073903–073903-5.

Duft, D., et al., 2003. Coulomb fission: Rayleigh jets from levitated microdroplets. Nature 421 (6919), 128.

Dumont, Q., Cole, R.B., 2013. Jean-Antoine Nollet: the farther of experimental electrospray. Mass Spectrom. Rev. , http://dx.doi.org/10.1002/mas.21397.

Duong, A.D., et al., 2013. Electrospray encapsulation of toll-like receptor agonist resiquimod in polymer microparticles for the treatment of visceral leishmaniasis. Mol. Pharm. 10 (3), 1045–1055.

Duong, A.D., et al., 2014. Scalable, semicontinuous production of micelles encapsulating nanoparticles via electrospray. Langmuir , http://dx.doi.org/10.1021/la404679r.

Eltayeb, M., et al., 2013. Preparation of solid lipid nanoparticles containing active compound by electrohydrodynamic spraying. Food Res. Int. 53 (1), 88–95.

Enayati, M., et al., 2010. Size mapping of electric field-assisted production of polycaprolactone particles. J. R. Soc. Interface 7 (Suppl. 4), S393–S402.

Fantini, D., et al., 2006. Polystyrene microspheres and nanopheres produced by electrospray. Macromol. Rapid Commun. 27 (23), 2038–2042.

Farook, U., et al., 2007a. Microbubbling by co-axial electrohydrodynamic atomization. Med. Biol. Eng. Comp. 45 (8), 781–789.

Farook, U., et al., 2007b. Preparation of microbubble suspensions by co-axial electrohydrodynamic atomization. Med. Eng. Phys. 29 (7), 749–754.

Farook, U., et al., 2009. Preparation of suspensions of phospholipid-coated microbubbles by coaxial electrohydrodynamic atomization. J. R. Soc. Interface 6 (32), 271–277.

Fenn, J.B., 1989. Electrospray ionization for mass spectrometry of large biomolecules. Science 246 (4926), 64–71.

Francis, L., et al., 2010. Simultaneous electrospin–electrosprayed biocomposite nanofibrous scaffolds for bone tissue regeneration. Acta Biomater. 6 (10), 4100–4109.

Freiberg, S., Zhu, X., 2004. Polymer microspheres for controlled drug release. Int. J. Pharm. 282 (1–2), 1–18.

Fu, H., et al., 2012. Performance study of a twin-head electrospray system. J. Aerosol Sci. 52, 33–44.

Galliker, P., et al., 2011. Direct printing of nanostructures by electrostatic autofocussing of ink nanodroplets. Nat. Commun. 3, 1–9.

Ganan-Calvo, A.M., et al., 1994. The electrostatic spray emitted from an electrified conical meniscus. J. Aerosol Sci. 25 (6), 1121–1142.

Ganan-Calvo, A.M., 1997. Cone-jet analytical extension of Taylor's electrostatic solution and the asymptotic universal scaling laws in electrospraying. Phys. Rev. Lett. 79 (2), 217.

Ganan-Calvo, A.M., et al., 1997. Current and droplet size in the electrospraying of liquids. scaling laws. J. Aerosol Sci. 28 (2), 249–275.

Ganan-Calvo, A.M., et al., 2003. The minimum or natural rate of flow and droplet size ejected by Taylor cone-jets: physical symmetries and scaling laws. New. J. Phys. 15, 033035.
Ganan-Calvo, A.M., 2004. On the general scaling theory for electrospraying. J. Fluid Mech. 507, 203–212a.
Gasperini, L., et al., 2013. Microencapsulation of cells in alginate through an electrohydrodynamic process. J. Bioact. Compat. Polym. 28 (5), 413–425.
Gaury, J., et al., 2013. Characterization of Nb-doped $WO_3$ thin films produced by Electrostatic Spray Deposition. Thin Solid Films 534 (1), 32–39.
Geerse, K.B., 2003. Applications of Electrospray: From People to Plants (Ph.D. dissertation). Department of Chemical Technology, Delft University of Technology, The Netherlands.
George, M.C., Braun, P.V., 2009. Multicompartmental materials by electrohydrodynamic cojetting. Angew. Chem. Int. Ed. 48 (46), 8606–8609.
Ghimbeu, M., et al., 2007. Preparation and characterization of $SnO_2$ and Cu-doped $SnO_2$ thin films using electrostatic spray deposition ESD. J. Eur. Ceram. Soc. 27 (1), 207–213.
Ghimbeu, M., et al., 2009. Electrosprayed metal oxide semiconductor films for sensitive and selective detection of hydrogen sulfide. Sensors 9 (11), 9122–9132.
Gilbert William of Colchester (Gvilielmi Gilberti). – De Magnete. –Londini, Anno MDC, 1600.
Gomez, A., et al., 1998. Production of protein nanoparticles by electrospray drying. J. Aerosol Sci. 29 (5), 561–574.
Gomez, A., Tang, K., 1994. Charge and fission of droplets in electrostatic sprays. Phys. Fluids 6 (1), 404–414.
Gomez-Estaca, J., et al., 2012. Formation of zein nanoparticles by electrohydrodynamic atomization: effect of the main processing variables and suitability for encapsulating the food coloring and active ingredient curcumin. Food Hydrocoll. 28 (1), 82–91.
Goosen, M.F.A., et al., 1997. Electrostatic droplet generation for encapsulation of somatic tissue: assessment of high-voltage power supply. Biotechnol. Prog. 13 (4), 497–502.
Gorty, A.V., Barringer, S.A., 2011. Electrohydrodynamic spraying of chocolate. J. Food Process. Preserv. 35 (4), 542–549.
Grafahrend, E., et al., 2010. Development and optimization of an electrospraying device for the continuous collection of nano- and microparticles. Open Chem. Biochem. Methods J. 3 (1), 1–9.
Grayson, M.A., 2011. John Bennett Fenn: a curious road to the prize. J. Am. Soc. Mass Spectrom. 22 (8), 1301–1308.
Gu, Z., et al., 2013. Injectable nano-network for glucose-mediated insulin delivery. ACS Nano 7 (5), 6758–6766.
Gun, S., et al., 2013. Encapsulation of superparamagnetic iron oxide nanoparticles in poly-(lactide-co-glycolic acid) microspheres for biomedical applications. Mater. Sci. Eng. C Mater. Biol. Appl. 33 (6), 3129–3137.
Guo, X., et al., 2014. Electrosprayed microparticles with loaded pdna-calcium phosphate nanoparticles to promote the regeneration of mature blood vessels. Pharm. Res. 31 (4), 874–886.
Hartman, R.P.A., et al., 1999. Electrohydrodynamic atomization in the cone-jet mode physical modeling of the liquid cone and jet. J. Aerosol Sci. 30 (7), 823–849.
Hartman, R.P.A., et al., 2000. Jet break-up in electrohydrodynaminc atomization in the cone-jet mode. J. Aerosol Sci. 31 (1), 65–95.
Hayashi, K., et al., 2010. Electrosprayed synthesis of red-blood-cell-like particles with dual modality for magnetic resonance and fluorescence imaging. Small 6 (21), 2384–2391.
Hazeri, N., et al., 2012. Production and properties of electrosprayed sericin nanopowder. Sci. Technol. Adv. Mater. 13 (3), 035010.
Higashi, K., et al., 2014. Micropatterning of silica nanoparticles by electrospray deposition through a stencil mask. J. Lab. Autom. 19 (1), 75–81.
Hirt, C.W., Nichols, B.D., 1981. Volume of fluid (VOF) method for the dynamics of free boundaries. J. Comput. Phys. 39 (1), 201–225.
Hohman, M.M., et al., 2001. Electrospinning and electrically forced jets. II. Applications. Phys. Fluid 13 (8), 2221–2236.
Hua, J.S., Lou, J., 2007. Numerical simulation of bubble rising in viscous liquid. J. Comput. Phys. 222 (2), 769–795.
Huang, L.Y., et al., 2012. Sustained release of ethyl cellulose micro-particulate drug delivery systems prepared using electrospraying. J. Mater. Sci. 47, 1372–1377.
Hwang, S., et al., 2010. Anisotropic hybrid particles based on electrohydrodynamic co-jetting of nanoparticle suspensions. Phys. Chem. Chem. Phys. 12 (38), 11894–11899.
Hyuncheol, O., et al., 2007. Synthesis of ceria nanoparticles by flame electrospray pyrolysis. J. Aerosol Sci. 38 (12), 1185–1196.
Ijsebaert, J.C., et al., 2001. Electro-hydrodynamic atomization of drug solutions for inhalation purposes. J. Appl. Physiol. 91 (6), 2735–2741.
Ikeuchi, M., et al., 2012. Electrospray deposition and direct patterning of polylactic acid nanofibrous microcapsules for tissue engineering. Biomed. Microdevices 14 (1), 35–43.
Jacobs-Tulleneers-Thevissen, D., et al., 2013. Sustained function of alginate-encapsulated human islet cell implants in the peritoneal cavity of mice leading to a pilot study in a type 1 diabetic patient. Diabetologia 56, 1605–1614.
Jennerjohn, N., et al., 2010. Design, demonstration and performance of a versatile electrospray aerosol generator for nanomaterial research and applications. Nanotechnology 21 (25), 255603.
Joki, T., et al., 2001. Continuous release of endostatin from microencapsulated engineered cells for tumor therapy. Nat. Biotechnol. 19 (1), 35–39.
Jung, J.H., et al., 2010. Numerical simulation of the deposition pattern in multiple electrohydrodynamic spraying. Powder Technol. 198 (3), 439–444.
Kachouie, N.N., et al., 2010. Direct assembly of cell-laden hydrogels for engineering functional tissues. Organogenesis 6 (4), 234–244.
Kandjani, E.A., et al., 2010. Powder production via electrohydrodynamic-assisted molten metal jet impingement into a viscous medium. Powder Technol. 203 (3), 518–528.
Kanev, L.L., et al., 2014. Are reactive oxygen species generated in electrospray at low currents? Anal. Chem. 86 (3), 1511–1517.
Kawakami, K., 2012. Miscibility analysis of particulate solid dispersions prepared by electrospray deposition. Int. J. Pharm. 433 (1–2), 71–78.
Kazemi, A., Lahann, L., 2008. Environmentally responsive core/shell particles via electrohydrodynamic co-jetting of fully miscible polymer solutions. Small 4 (10), 1756–1762.
Kim, H., et al., 2006. Parallel patterning of nanoparticles via electrodynamic focusing of charged aerosols. Nat. Nanotechnol. 1 (2), 117–121.
Kim, J.H., et al., 2009. Direct pattern formation of bacterial cells using microdroplets generated by electrohydrodynamic forces. Microfluid Nanofluid 7 (6), 829–839.
Kim, K., et al., 2010a. Drop-on-demand patterning of bacterial cells using pulsed jet electrospraying. Anal. Chem. 82 (5), 2109–2112.
Kim, S., et al., 2013. Continuous coaxial electrohydrodynamic atomization system for water-stable wrapping of magnetic nanoparticles. Small 9 (13), 2325–2330.
Kim, W., Kim, S., 2010. Multishell encapsulation using a triple coaxial electrospray system. Anal. Chem. 82 (11), 4644–4647.
Kim, S., et al., 2010b. A nanoparticle dispersion method for in vitro and in vivo nanotoxicity study. Nanotoxicology 4 (1), 42–51.
Korkut, S., et al., 2008. Colloidal cluster arrays by electrohydrodynamic printing. Langmuir 24 (21), 12196–12201.
Koshkina, N.V., et al., 2003. Biodistribution and pharmacokinetics of aerosol and intravenously administered DNA–polyethyleneimine complexes: optimization of pulmonary delivery and retention. Mol. Ther. 8, 249–254.
Labbaf, S., et al., 2013. Preparation of multicompartment sub-micron particles using a triple-needle electrohydrodynamic device. J. Colloid Interface Sci. 409 (1), 245–254.
Lahann, J., et al., 2011. Recent progress in nano-biotechnology: compartmentalized micro- and nanoparticles via electrohydrodynamic co-jetting. Small 7 (9), 1149–1156.
Lastow, O., Balachandran, W., 2006. Numerical simulation of electrohydrodynamic (EHD) atomization. J. Electrostat. 64 (12), 850–859.
Lee, D., et al., 2007. Electrohydrodynamic printing of silver nanoparticles by using a focused nanocolloid jet. Appl. Phys. Lett. 90 (8), 081905.
Lee, H., et al., 2011a. Three-dimensional assembly of nanoparticles from charged aerosols. Nano Lett. 11 (1), 119–124.
Lee, J.S., 2013. Multidimensional polypyrrole/iron oxyhydroxide hybrid nanoparticles for chemical nerve gas agent sensing application. ACS Nano 7 (11), 10139–10147.
Lee, J.S., et al., 2014. Urchin-like polypyrrole nanoparticles for highly sensitive and selective chemiresistive sensor application. Nanoscale 6 (8), 4188–4194.
Lee, K.H., et al., 2003. The change of bead morphology formed on electrospun polystyrene fibers. Polymer 44 (14), 4029–4034.
Lee, S.Y., et al., 2010a. Osseointegration of anodized titanium implants coated with poly(lactide-co-glycolide)/basic fibroblast growth factor by electrospray. Int. J. Oral Maxillofac. Implants 25 (2), 315–320.
Lee, Y., et al., 2010b. Release profile characteristics of biodegradable-polymer-coated drug particles fabricated by dual-capillary electrospray. J. Control. Rel. 145 (1), 58–65.
Lee, Y., et al., 2011b. Multidrug encapsulation by coaxial tri-capillary electrospray. Colloids Surf. B: Biointerfaces 82 (1), 104–110.
Lee, Y., et al., 2011c. Nanoparticles facilitate gene delivery to microorganisms via an electrospray process. J. Microbiol. Methods 84 (2), 228–233.
Lenggoro, I.W., et al., 2002. Sizing of colloidal nanoparticles by electrospray and differential mobility analyzer methods. Langmuir 18 (12), 4584–4591.
Lenggoro, I.W., et al., 2000. Preparation of ZnS nanoparticles by electrospray pyrolysis. J. Aerosol Sci. 31 (1), 121–136.
Levit, R.D., et al., 2013. Cellular encapsulation enhances cardiac repair. J. Am. Heart Assoc. 2, e000367.
Li, C., et al., 2014. Fast-dissolving core–shell composite microparticles of quercetin fabricated using a coaxial electrospray process. PLOS One , http://dx.doi.org/10.1371/journal.pone.0092106.
Li, S.W., et al., 2006. Aspirin particle formation by electric-field-assisted release of droplets. Chem. Eng. Sci. 61 (10), 3091–3097.
Li, X., et al., 2007. Electrohydrodynamic coating of metal with nano-sized hydroxyapatite. Bio-Med. Mater. Eng. 17 (6), 335–346.
Li, X., et al., 2008. Novel patterning of nano-bioceramics: template-assisted electrohydrodynamic atomization spraying. J. R. Soc. Interface 5 (19), 253–257.
Li, X., et al., 2010. Fabrication of density gradients of biodegradable polymer microparticles and their use in guiding neurite outgrowth. Adv. Funct. Mater. 20 (10), 1632–1637.
Lim, D.W., et al., 2010. Compartmentalization of gold nanocrystals in polymer microparticles using electrohydrodynamic co-jetting. Macromol. Rapid Commun. 31 (2), 176–182.
Lim, L.K., et al., 2011. Numerical simulation of cone-jet formation in electrohydrodynamic atomization. AIChE J. 57 (1), 57–78.
Liu, J., Kumar, S., 2005. Microscopic polymer cups by electrospinning. Polymer 46 (10), 3211–3214.

Liu, J., Nguyen, N.T., 2010. Numerical simulation of droplet-based microfluidics—a review. Micro Nanosyst. 2 (3), 1876–4037.
Loscertales, G., et al., 2002. Micro/nano encapsulation via electrified coaxial liquid. Science 295 (5560), 1695–1698.
Luo, C.J., et al., 2012. Electrospraying and electrospinning of chocolate suspensions. Food Bioprocess Technol. 5 (6), 2285–2300.
Ma, et al., 2013. Core–shell hydrogel microcapsules for improved islets encapsulation. Adv. Healthcare Mater. 2 (5), 667–672.
Marthina, K., Barringer, S.A., 2012. Confectionery coating with an electrohydrodynamic (EHD) system. J. Food Sci. 77 (1), E26–E31.
Martyn, S.V., et al., 2011. Electrospray deposited fibronectin retains the ability to promote cell adhesion. J. Biomed. Mater. Res. B Appl. Biomater. 96B (1), 110–118.
Mastel, A.J., 1994. Electrohydrodynamic stability of a slightly viscous jet. J. Fluid Mech. 274, 93–113.
Materi, C., et al., 2007. Preparation and characterization of $SnO_2$ and Cu-doped $SO_2$ thin films using electrostatic spray deposition (ESD). J. Eur. Ceram. Soc. 27 (1), 207–213.
Materi, C., et al., 2009. Electrosprayed metal oxide semiconductor films for sensitive and selective detection of hydrogen sulfide. Sensors 9 (11), 9122–9132.
Matsushima, Y., et al., 2004. Fabrication of $SnO_2$ particle-layers using the electrospray method and gas sensing properties for $H_2$. J. Electroceram. 13 (1), 765–770.
Misra, A.C., et al., 2012. Multicompartmental particles for combined imaging and siRNA delivery. Adv. Mater. 24 (28), 3850–3856.
Modesto-Lopez, L.B., Biswas, P., 2010. Role of the effective electrical conductivity of nanosuspensions in the generation of $TiO_2$ agglomerates with electrospray. J. Aerosol Sci. 41 (8), 790–804.
Moghadam, H., et al., 2008. Electro-spray of high viscous liquids for producing mono-sized spherical alginate beads. Particuology 6 (4), 271–275.
Mongkoldhumrongkul, N., et al., 2010. Bio-electrospraying the nematode Caenorhabditis elegans: studying whole-genome transcriptional responses and key life cycle parameters. J. R. Soc. Interface 7 (45), 595–601.
Moon, J.H., et al., 2004. Electrospray-assisted fabrication of uniform photonic balls. Adv. Mater. 16 (7), 605–609.
Morozov, V.N., 2011. Generation of biologically active nano-aerosol by an electrospray-neutralization method. J. Aerosol Sci. 42 (5), 341–354.
Morozov, V.N., Morozova, T.Y., 1999. Electrospray deposition as a method to fabricate functionally active protein films. Anal. Chem. 71 (7), 1415–1420.
Morozov, V.N., 2010. Electrospray deposition of biomolecules. Adv. Biochem. Eng. Biotechnol. 119, 115–162.
Morozov, V.N., Morozova, T.Y., 1999. Electrospray deposition as a method for mass fabrication of mono- and multicomponent microarrays of biological and biologically active substances. Anal. Chem. 71 (15), 3110–3117.
Mou, F., et al., 2013. Oppositely charged twin-head electrospray: a general strategy for building Janus particles with controlled structures. Nanoscale 5 (5), 2055–2064.
Munir, G., et al., 2011. The pathway to intelligent implants: osteoblast response to nano silicon-doped hydroxyapatite patterning. J. R. Soc. Interface 8 (58), 678–688.
Naraharisetti, P.K., et al., 2007. In vivo performance of implantable biodegradable preparations delivering Paclitaxel and Etanidazole for the treatment of glioma. Biomaterials 28 (5), 886–894.
Nayyar, N.K., Murty, G.S., 1960. The stability of a dielectric liquid in the presence of a longitudinal electric field. Proc. Phys. Soc. Lond. 75 (3), 369–373.
Ng, K., et al., 2011. Bio-electrospraying primary cardiac cells: in vitro tissue creation and functional study. Biotechnol. J. 6 (1), 86–95.
Nie, H., et al., 2010a. Core/shell microspheres via coaxial electrohydrodynamic atomization for sequential and parallel release of drugs. J. Biomed. Mater. Res. A 95 (3), 709–716.
Nie, H., et al., 2010b. Paclitaxel and suramin-loaded core/shell microspheres in the treatment of brain tumors. Biomaterials 31 (33), 8732–8740.
Nithyanandan, A., et al., 2013. Template-assisted electrohydrodynamic atomization of polycaprolactone for orthopedic patterning applications. Mater. Biol. Appl. 33 (8), 4608–4615.
Nystrom, M., et al., 2011. Fabrication of amorphous pharmaceutical materials by electrospraying into reduced pressure. J. Electrostat. 69 (4), 351–356.
Okubo, K., et al., 2008. DNA introduction into living cells by water droplet impact with an electrospray process. Angew. Chem. Int. Ed. 47 (8), 1429–1431.
Oh, H., Kim, S., 2007. Synthesis of ceria nanoparticles by flame electrospray pyrolysis. J. Aerosol Sci. 38 (12), 1185–1196.
Pancholi, K., et al., 2007. Novel methods for preparing phospholipid coated microbubbles. Eur. Biophys. J. 37 (4), 515–520.
Pancholi, K., et al., 2009. Novel electrohydrodynamic preparation of porous chitosan particles for drug delivery. J. Mater. Sci.: Mater. Med. 20 (4), 917–923.
Pareta, R., Edirisinghe, M.J., 2006. A novel method for the preparation of biodegradable microspheres for protein drug delivery. J. R. Soc. Interface 3 (9), 573–582.
Park, C.H., et al., 2011. Monodisperse red blood cell-like particles via consolidation of charged droplets. J. Colloid Interface Sci. 361 (2), 423–428.
Park, D.G., Burlith, J.M., 1992. Nanoparticles of anatase by electrostatic spraying of an alkoxide solution. Chem. Mater. 4 (3), 500–502.
Park, D.G., Burlith, J.M., 1996. Electro-spray synthesis of titanium oxide nanoparticles. J. Sol–Gel Sci. Technol. 6 (3), 235–249.
Park, H., et al., 2012a. Fabrication of cross-linked alginate beads using electrospraying for adenovirus delivery. Int. J. Pharm. 427 (2), 417–425.
Park, J.H., et al., 2012b. Poly(vinyl alcohol)/montmorillonite/silver hybrid nanoparticles prepared from aqueous solutions by the electrospraying method. J. Compos. Mater. 47 (27), 3367–3378.
Park, J.H., et al., 2013. Poly(vinyl alcohol)/montmorillonite/silver hybrid nanoparticles prepared from aqueous solutions by the electrospraying method. J. Compos. Mater. 47 (27), 3367–3378.
Park, J.U., et al., 2007. High-resolution electrohydrodynamic jet printing. Nat. Mater. 6 (10), 782–789.
Park, J.U., et al., 2008. Nanoscale patterns of oligonucleotides formed by electrohydrodynamic jet printing with applications in biosensing and nanomaterials assembly. Nano Lett. 8 (12), 4210–4216.
Park, S.M., et al., 2011. Preparation of low molecular weight poly(vinyl alcohol)/montmorillonite composite nanoparticles using an electrospraying technique. Polym. Polym. Compos. 19 (1), 35–40.
Pengpong, T., et al., 2014. Design, synthesis and in vitro evaluation of mucoadhesive p-coumarate-thiolated-chitosan as a hydrophobic drug carriers. J. Pharm. Biopharm. 86 (3), 487–497.
Poon, H.F., et al., 2008. Linear colloidal crystal arrays by electrohydrodynamic printing. Appl. Phys. Lett. 93 (13), 133114–133114-3.
Radacsi, N., et al., 2012. Electrospray crystallization for nanosized pharmaceuticals with improved properties. Cryst. Growth Des. 12 (7), 3514–3520.
Rahman, K., et al., 2012. Fine-resolution patterning of copper nanoparticles through electrohydrodynamic jet printing. J. Micromech. Microeng. 22 (6), 065012–065018.
Rahmani, S., et al., 2013. Multimodal delivery of irinotecan from microparticles with two distinct compartments. J. Control. Rel. 172 (1), 239–241.
Ranganath, H., et al., 2009a. Hydrogel matrix entrapping PLGA-paclitaxel microspheres: drug delivery with near zero-order release and implantability advantages for malignant brain tumour chemotherapy. Pharm. Res. 26 (9), 2101–2114.
Ranganath, H., et al., 2009b. The use of submicron/nanoscale PLGA implants to deliver paclitaxel with enhanced pharmacokinetics and therapeutic efficacy in intracranial glioblastoma in mice. Biomaterials 31 (19), 5199–5207.
Rayleigh, L., 1882. On the equilibrium of liquid conducting masses charged with electricity. Philos. Mag. 14, 184–186.
Regele, J.D., et al., 2002. Effects of capillary spacing on EHD spraying from an array of cone jets. J. Aerosol Sci. 33 (11), 1471–1479.
Rezvanpour, A., et al., 2010. Enhancement of particle collection efficiency in Electrohydrodynamic atomization process for pharmaceutical particle fabrication. Ind. Eng. Chem. Res. 49 (24), 12620–12631.
Rezvanpour, A., et al., 2012. Scaling analysis of the electrohydrodynamic atomization (EHDA) process for pharmaceutical particle fabrication. Chem. Eng. Sci. 80 (1), 81–90.
Rezvanpour, A., Wang, C.H., 2011. Computational and experimental studies of electrospray deposition process in pharmaceutical micro-pattern formation. Chem. Eng. Sci. 66 (17), 3836–3849.
Rezvanpour, A., Wang, C.H., 2014. The effects of auxiliary electric field within the electrohydrodynamic atomization encapsulation chamber on particle size, morphology and collection efficiency. Chem. Eng. J. 239 (1), 8–18.
Roh, K., et al., 2005. Biphasic janus particles with nanoscale anisotropy. Nat. Mater. 4 (10), 759–763.
Roh, K., et al., 2006. Triphasic nanocolloids. J. Am. Chem. Soc. 128 (21), 6796–6797.
Roh, K., et al., 2007. Water-stable biphasic nanocolloids with potential use as anisotropic imaging probes. Langmuir 23 (10), 5683–5688.
Rulison, A.J., Flagan, R.C., 1993. Scaleup of electrospray atomization using linear arrays of Taylor cones. Rev. Sci. Instrum. 64 (3), 683–686.
Saf, Q., et al., 2004. Thin organic films by atmospheric-pressure ion deposition. Nat. Mater. 3, 323–329.
Sahoo, S., et al., 2010. Bio-electrospraying: A potentially safe technique for delivering progenitor cells. Biotechnol. Bioeng. 106 (4), 690–698.
Salata, O.V., 2005. Tools of nanotechnology: electrospray. Curr. Nanosci. 1, 25–33.
Samarasinghe, S.R., et al., 2006. Electric-jet assisted layer-by-layer deposition of gold nanoparticles to prepare conducting tracks. Gold Bull. 39 (2), 48–53.
Saville, D.A., 1970. Electrohydrodynamic stability: fluid cylinders in longitudinal electric fields. Phys. Fluid 13 (12), 2987–2994.
Saville, D.A., 1971a. Stability of electrically charged viscous cylinders. Phys. Fluid 14, 1095–1099.
Saville, D.A., 1971b. Electrohydrodynamic stability: effects of charge relaxation at the interface of a liquid jet. J. Fluid Mech. 48 (4), 815–827.
Saywell, A., et al., 2010. Conformation and packing of porphyrin polymer chains deposited using electrospray on a gold surface. Angew. Chem. Int. Ed. 49 (48), 9136–9139.
Scheideler, W.J., Chen, C.H., 2014. The minimum flow rate scaling of Taylor cone-jets issued from a nozzle. Appl. Phys. Lett. 104, 024103.
Scholten, E., et al., 2011. Electrospray as a tool for drug micro- and nanoparticle patterning. Langmuir 27 (11), 6683–6688.
Sengupta, S., et al., 2005. Temporal targeting of tumour cells and neurovasculature with a nanoscale delivery system. Nature 436, 568–572.
Seth, A., Katt, D.S., 2012. A one-step electrospray-based technique for modulating morphology and surface properties of poly(lactide-co-glycolide) microparticles using Pluronics. Int. J. Nanomed. 7, 5129–5136.
Shen, Z., et al., 2010. Fabrication of robust crystal balls from the electrospray of soft polymer spheres/silica dispersion. Langmuir 26 (9), 6604–6609.
Shenoy, S.L., et al., 2005. Role of chain entanglements on fiber formation during electrospinning of polymer solutions: good solvent, non-specific polymer–polymer interaction limit. Polymer 46 (10), 3372–3384.

Shim, I., et al., 2013. Biofunctional porous anodized titanium implants for enhanced bone regeneration. J. Biomed. Mater. Res. A , http://dx.doi.org/10.1002/jbm.a.35026.
Shtern, V., Barrero, A., 1994. Striking features of fluid flows in taylor cones related to electrosprays. J. Aerosol Sci. 25 (6), 1049–1063.
Si, T., et al., 2012. Coaxial electrospray for multimodal imaging and image-guided therapy. In: Proceedings of SPIE 8216, Multimodal Biomedical Imaging VII, 82160M http://dx.doi.org/10.1117/12.909383.
Si, T., et al., 2013. Experimental design and instability analysis of coaxial electrospray process for microencapsulation of drugs and imaging agents. J. Biomed. Opt. 18 (7), 075003.
Sigmond, R.S., 1982. Simple approximate treatment of unipolar space-charge-dominated coronas: the Warburg law and the saturation current. J. Appl. Phys. 53 (2), 891–898.
Slavov, V., Dimova, S., 2007. Phase-field versus level set method for 2D dendritic growth. Numer. Methods Appl. 4310, 717–725.
Smith, D.P.H., 1986. The electrohydrodynamic atomization of liquids. IEEE Trans. Ind. Appl. 22 (3), 527–535.
Smith, J.N., 2000. Fundamental Studies of Droplet Evaporation and Discharge Dynamics in Electrospray Ionization (Ph.D. dissertation). California Institute of Technology.
Songsurang, K., et al., 2011. Electrospray fabrication of doxorubicin-chitosan-tripolyphosphate nanoparticles for delivery of doxorubicin. Arch. Pharm. Res. 34 (4), 583–592.
Stankus, J.J., et al., 2007. Fabrication of cell microintegrated blood vessel constructs through electrohydrodynamic atomization. Biomaterials 28 (17), 2738–2746.
Suksamran, T., et al., 2013. Methylated N-(4-N,N-dimethylaminocinnamyl) chitosan-coated electrospray OVA-loaded microparticles for oral vaccination. Int. J. Pharm. 448 (1), 19–27.
Sun, L., et al., 2011. Preparation of quantum dots encoded microspheres by electrospray for the detection of biomolecules. J. Colloid Interface Sci. 358 (1), 73–80.
Tabeei, A., et al., 2012. Study pulsating electrospray of non-newtonian and thixotropic sodium alginate solution. J. Electrostatics 70 (1), 77–82.
Tang, G.W., et al., 2013. Preparation of fiber-microsphere scaffolds for loading bioactive substances in gradient amounts. Chin. Sci. Bull. 58 (27), 3415–3421.
Tang, K., Gomez, J., 1994. Generation by electrospray of monodisperse water droplets for targeted drug delivery by inhalation. J. Aerosol Sci. 25 (6), 1237–1249.
Tavares Cardoso, M.A., et al., 2011. Functionalization of lactose as a biological carrier for bovine serum albumin by electrospray. Int. J. Pharm. 414 (1-2), 1–5.
Taylor, G., 1964. Disintegration of water drops in an electric field. Proc. R. Soc. Lond. A 280 (1382), 383–397.
Taylor, G.I., 1969. Electrically driven jets. Proc. R. Soc. A 313 (1515), 453–475.
Taylor, G., 1966. The force exerted by an electric field on a long cylindrical conductor. Proc. R. Soc. A 291 (1452), 145–158.
Terada, Y., et al., 2012. Synthesis and characterization of $TiO_2$ powders by electrospray pyrolysis method. Mater. Res. Bull. 47 (3), 889–895.
Tian, Y., et al., 2013. Novel erythrocyte-like graphene microspheres with high quality and mass production capability via electrospray assisted self-assembly. Sci. Rep. 3 (3327), 1–6.
Valo, H., et al., 2009. Electrospray encapsulation of hydrophilic and hydrophobic drugs in poly(L-lactic acid) nanoparticles. Small 5 (15), 1791–1798.
Wang, H., et al., 2013a. Electrospray formation of gelled nano-aluminum microspheres with superior reactivity. ACS Appl. Mater. Interfaces 5 (15), 6797–6801.
Wang, W., et al., 2005. One-step synthesis of titanium oxide nanoparticles by spray pyrolysis of organic precursors. Mater. Sci. Eng. B 123 (3), 194–202.
Wang, Y., et al., 2013b. Controlled release behavior of protein-loaded microparticles prepared via coaxial or emulsion electrospray. J. Microencapsul. 30 (5), 490–497.
Wang, J., Pui, Y.H., 2013. Dispersion and filtration of carbon nanotubes (CNTs) and measurement of nanoparticle agglomerates in diesel exhaust. Chem. Eng. Sci. 85 (14), 69–76.
Wang, M., et al., 2012. Production and characterization of carbamazepine nanocrystals by electrospraying for continuous pharmaceutical manufacturing. J. Pharm. Sci. 101 (3), 1178–1188.
Wihelm, O., et al., 2003. Electrospray evaporation and deposition. J. Aerosol Sci. 34 (7), 815–836.
Woo, C.G., et al., 2011. Selective nanopatterning of protein via ion-induced focusing and its application to metal-enhanced fluorescence. Small 7 (13), 1790–1794.
Woodruff, M.A., Hutmacher, D.W., 2010. The return of a forgotten polymer-polycaprolactonein 21st century. Prog. Polym. Sci. 35 (10), 1217–1256.
Wu, Y., et al., 2009a. Coaxial electrohydrodynamic spraying: a novel one-step technique to prepare oligodeoxynucleotide encapsulated lipoplex nanoparticles. Mol. Pharm. 6 (5), 1371–1379.
Wu, Y., et al., 2009b. Fabrication of elastin-like polypeptide nanoparticles for drug delivery by electrospraying. Biomacromolecules 10 (1), 19–24.
Wu, Y., et al., 2010a. Coaxial electrohydrodynamic spraying of plasmid DNA/polyethylenimine (PEI) polyplexes for enhanced nonviral gene delivery. Biotechnol. Bioeng. 105 (4), 834–841.
Wu, Y., et al., 2010b. Electrosprayed core–shell microspheres for protein delivery. Chem. Commun. 46 (26), 4743–4745.
Wu, Y., Clark, R.L., 2007. Controllabe porous polymer particles generated by electrospraying. J. Colloid Interface Sci. 310 (2), 529–535.
Xi, J., et al., 2011. Fabrication of $TiO_2$ aggregates by electrospraying and their application in dye-sensitized solar cells. Nanosci. Nanotechnol. Lett. 3 (5), 690–696.
Xie, J., et al., 2008a. Encapsulation of protein drugs in biodegradable microparticles by co-axial electrospray. J. Colloid Interface Sci. 317 (2), 469–476.
Xie, J., Wang, C.H., 2007a. Encapsulation of proteins in biodegradable polymeric microparticles using electrospray in the Taylor cone-jet mode. Biotech. Bioeng. 97 (5), 1278–1290.
Xie, J., et al., 2006a. Electrohydrodynamic atomization for biodegradable polymeric particle production. J. Colloid Interface Sci. 302 (1), 103–112.
Xie, J., et al., 2006b. Microparticles developed by electrohydrodynamic atomization for the local delivery of anticancer drug to treat C6 glioma in vitro. Biomaterials 27 (17), 3321–3332.
Xie, J., et al., 2010. Electric field controlled electrospray deposition for precise particle pattern and cell pattern formation. AIChE J. 56 (10), 2607–2621.
Xie, J., Wang, C.H., 2007b. Electrospray in the dripping mode for cell microencapsulation. J. Colloid Interface Sci. 312 (2), 247–255.
Xie, J., et al., 2008b. Biodegradable microparticles and fiber fabrics for sustained delivery of cisplatin to treat C6 glioma in vitro. J. Biomed. Mater. Res. A 85 (4), 897–908.
Xu, Q., et al., 2013a. Coaxial electrohydrodynamic atomization process for production of polymeric composite microspheres. Chem. Eng. Sci. 104 (18), 330–346.
Xu, S., et al., 2013b. Preparation and characterization of folate-chitosan-gemcitabine core–shell nanoparticles for potential tumor-targeted drug delivery. J. Nanosci. Nanotechnol. 13 (1), 129–138.
Xu, Y., et al., 2006. Electrospray encapsulation of water-soluble protein with polylactide. I. Effects of formulations and process on morphology and particle size. J. Microencapsul. 23 (1), 69–78.
Yan, F., et al., 2003. Numerical modeling of an electrostatically driven liquid meniscus in the cone-jet mode. J. Aerosol Sci. 34 (1), 99–116.
Yang, Y., et al., 1993. The effects of particles on the stability of two-phase wake flows. Int. J. Multiph. Flow 19 (1), 137–149.
Yeo, L.Y., et al., 2005. AC electrospray biomaterials synthesis. Biomaterials 26 (31), 6122–6128.
Yoshida, M., et al., 2009. Structurally controlled bio-hybrid materials based on unidirectional association of anisotropic microparticles with human endothelial cells. Adv. Mater. 21 (48), 4920–4925.
Young, C.J., et al., 2012. Combining submerged electrospray and UV photopolymerization for production of synthetic hydrogel microspheres for cell encapsulation. Biotechnol. Bioeng. 109 (6), 1561–1570.
Yu, X., Hu, Z., 1997. Production of nanometer powders with an electrohydrodynamic technique. J. Mater. Sci. Technol. 13 (3), 211–214.
Yun, K.M., et al., 2009. A new physical route to produce monodispersed microsphere nanoparticle–polymer composites. Langmuir 25 (18), 11038–11042.
Zeleny, J., 1917. Instability of electrified liquid surfaces. Phys. Rev. 10 (1), 1–6.
Zhang, S., et al., 2011. Coaxial electrospray formulations for improving oral absorption of a poorly water-soluble drug. Mol. Pharm. 8 (3), 807–813.
Zhang, S., Kawakami, K., 2010. One-step preparation of chitosan solid nanoparticles by electrospray deposition. Int. J. Pharm. 397 (1–2), 211–217.
Zhang, W., et al., 2013. A novel core–shell microcapsules for encapsulation and 3D culture of embryonic stem cells. J. Mater. Chem. B Mater. Biol. Med. 2013 (7), 1002–1009.
Zhao, Y., Jiang, L., 2009. Hollow micro/nanomaterials with multilevel interior structures. Adv. Mater. 21 (36), 3621–3638.